Engineering Structures 353 (2026) 122162

Contents lists available at ScienceDirect

Engineering Structures

journal homepage: www.elsevier.com/locate/engstruct

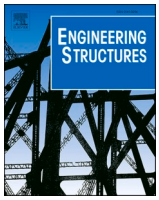

Numerical study of RC frames with decoupled masonry infills with and without openings under in-plane seismic loads

Aleksa Milijaš [a,*], Marko Marinković [b], Christoph Butenweg [c], Sven Klinkel [a]

[a] Chair of Structural Analysis and Dynamics, RWTH Aachen University, Mies-van-der-Rohe-Straße 1, 52074 Aachen, Germany
[b] Chair of Engineering Mechanics and Theory of Structures, Faculty of Civil Engineering, University of Belgrade, Bulevar kralja Aleksandra 73, 11000 Belgrade, Serbia
[c] FH Aachen – University of Applied Sciences, Heinrich-Mußmann-Straße 1, 52428 Jülich, Germany

ARTICLE INFO

Keywords:
Decoupling system
Simplified micro-model
Internal forces
Design concept
Eurocode 8

ABSTRACT

This study presents an innovative decoupling solution designed to improve the seismic performance of infilled reinforced concrete (RC) frame structures. Previous experimental research by the authors confirmed the effectiveness of the decoupling system through a series of full-scale separate and combined in-plane and out-of-plane tests. In the present work, a simplified micro-model developed and realised in Abaqus is validated against three experimental tests and then employed in a comprehensive parametric study investigating the in-plane behaviour of RC frames with decoupled masonry infills featuring various opening types (windows, doors and partial infills) of different sizes and locations. The results demonstrate that the decoupling system successfully reduces adverse frame-infill interaction effects across all configurations. The first cracks in the decoupled masonry infills are typically observed at in-plane drifts exceeding the maximum design in-plane drift of 2.0 %. Meanwhile, the in-plane response of the frames remains largely unaffected. Finally, based on the comprehensive findings of the study, and in accordance with the second generation of Eurocode 8, practical guidelines are proposed for the design of the novel decoupling system to ensure efficient decoupling of masonry infills from the RC frames.

1. Introduction

Reinforced concrete (RC) frames with traditionally constructed masonry infills are widely used in buildings around the world, especially in earthquake-prone areas. Specific to this type of structure is the frame-infill interaction that occurs under seismic loading. Although this interaction is neglected in most seismic codes, it plays a critical role in the seismic response of infilled frame structures, since it has been identified as a primary cause of extensive non-structural and structural damage, as well as building collapse, during recent earthquakes [1–4]. To better understand the complex frame-infill interaction, the in-plane behaviour of infilled frames has been investigated in numerous experimental studies (e.g. [5–9]). Comprehensive overviews of the experimental research are provided in recent state-of-the-art reviews [10,11] too. Furthermore, with advancements in computational methods, the seismic response of infilled frame structures has also been extensively investigated through numerical simulations. Various modelling approaches have been developed, which basically differ in the level of detail used to represent an infilled frame. According to [12], approaches based on the finite element method can be categorised by complexity into detailed and simplified micro-modelling, smeared homogenous (or "meso") modelling, and macro-modelling. The studies carried out using micro- [13–15] and "meso" [16–18] modelling techniques were mainly able to satisfactorily depict the experimental response of the infilled RC frames, in correspondence with the limitations of the respective modelling approach. Similarly, some investigations using the discrete element method [19,20] achieved a quite good agreement with experimental results. However, there is a significant gap in the research on the investigation of internal forces in RC frames, which is crucial for evaluating the effects of masonry infills on the surrounding frames. To date, this topic has been addressed only in a limited number of studies: [17,18] using "meso"-modelling, and [21,22] through micro-modelling technique. These investigations indicate that traditional masonry infills significantly alter the distribution of bending moments and shear forces in RC columns compared to those observed in the corresponding bare frame used in the design. In the macro-modelling approach, masonry infill is usually replaced by one concentric diagonal strut, e.g. [23,24]. A major disadvantage in this case is that the distribution of bending

* Corresponding author.
E-mail addresses: milijas@lbb.rwth-aachen.de (A. Milijaš), mmarinkovic@grf.bg.ac.rs (M. Marinković), christoph.butenweg@fh-aachen.de (C. Butenweg), klinkel@lbb.rwth-aachen.de (S. Klinkel).

https://doi.org/10.1016/j.engstruct.2026.122162
Received 14 August 2025; Received in revised form 2 January 2026; Accepted 11 January 2026
Available online 22 January 2026

moments and shear forces on the surrounding RC frame is not correctly determined, and thus, local effects cannot be evaluated. Therefore, in order to more appropriately evaluate the effect of the masonry infill on the surrounding RC frame, some authors propose macro-models with one eccentric diagonal strut [25,26] or several diagonal struts [27,28]. More recently, [29,30] proposed approaches that model the masonry infill as a concentric diagonal strut, and additionally take into account the effect of shear forces acting on the frame.

Despite extensive scientific efforts, the frame-infill interaction remains an intricate issue, and a simple and unified engineering approach to account for masonry infills in the seismic design is still missing. Even if directions for calculating the masonry infill in-plane stiffness or force capacity are provided – for example, in MSJC [31] and FEMA 306 [32], they are usually based on the simple diagonal strut models, which are prone to errors due to the large variability in material and geometric properties of infilled RC frames [33,34]. It can be concluded that there is an urgent need to improve the poor seismic performance of infilled RC frames by eliminating adverse frame-infill interaction effects, and to develop a reliable design approach for these structures.

A promising way to overcome the drawbacks of infilled RC frames is to decouple the masonry infill from the frame using a gap filled with a soft material [35,36]. While this approach has proven effective under in-plane loading, out-of-plane stability remains a concern. Some national codes [31,37,38] recommend using connectors to ensure out-of-plane safety, but experiments have shown significant deficiencies - such as connector failures during in-plane tests and stress-induced brick damage under combined loading [39,40]. Although newer decoupled masonry infill concepts show improved performance under combined loading, their installation is overly complex [41,42]. Overall, current decoupling methods suffer from three main issues: unreliable out-of-plane safety, poor seismic performance under combined loading, and complicated installation.

To address these limitations, the INODIS (Innovative Decoupled Infill System) was developed, demonstrating high seismic safety under combined in-plane and out-of-plane loading while maintaining installation simplicity [43]. Subsequent improvements optimised the layout of the system and incorporated recyclable rubber-based profiles bonded with mortar, enhancing sustainability and installation efficiency. Full-scale tests confirmed the improved seismic performance of the INODIS system [44].

However, a practical design framework for the INODIS system is still lacking. According to the second generation of Eurocode 8 (FprEN 1998–1–2:2025 [45]), such systems may be classified as non-interacting if their contribution to the in-plane stiffness and strength of structure is negligible. Therefore, the INODIS system must be designed to ensure minimal frame–infill interaction, approximating the behaviour of a bare RC frame as complete decoupling through an air gap is not feasible due to sound insulation requirements and out-of-plane stability concerns.

To address this issue, the in-plane behaviour of RC frames with INODIS decoupled masonry infills [44] is investigated through numerical simulations using a simplified micro-modelling approach [15]. The model is validated against three in-plane tests, followed by a comprehensive parametric study assessing the effectiveness of the system across various infill configurations and its compliance with the non-interacting criteria of FprEN 1998–1–2:2025 [45]. Particular attention is given to the influence of openings of different types, sizes, and locations, which are known to critically affect the in-plane response and seismic vulnerability of traditionally infilled frames [46,47] but remain unexplored for decoupled systems. The analyses compare force-drift responses, masonry infill activation, and damage patterns between infilled and bare frames, with particular focus on internal force distribution to assess the influence of masonry infills, an aspect rarely examined for traditional systems and unexplored for decoupled configurations. Finally, key in-plane response parameters, including stiffness, base shear, and column shear forces, are systematically evaluated across all configurations. Based on these findings, a design concept for RC frames with non-interacting masonry infills is proposed, consistent with FprEN 1998–1–2:2025 [45].

2. Decoupling system

The RC frames with decoupled masonry infills in this study refer to masonry infills decoupled from the RC frame by the decoupling system INODIS (Innovative Decoupled Infill System) presented in detail in [44]. Fig. 1 shows the concept of the system on a fully infilled RC frame, which was also experimentally tested in [44]. The columns have cross-sectional dimensions of 25 × 25 cm and the beam measures 45 cm in width and 25 cm in height. The concrete C30/37 and reinforcing steel B500B are used for the frame construction. Masonry infill measures 2.67 m in length, 2.5 m in height, and has a thickness of 30 cm. It is constructed using vertically perforated clay Thermoplan SX10 bricks. Only the bed joints are filled with thin-layer mortar Maxit mur 900D.

The decoupling system, installed between the masonry infill and RC frame, comprises three elastomeric strips made of recycled rubber. The middle strip is bonded to the RC frame, the outer strips to the bricks, using thin-layer mortar. In-plane deformations are accommodated by 50 mm thick, softer strips placed between the columns and masonry infill. Additionally, at the top of the masonry infill, thin plastic profiles with sliding surfaces are attached to the top surfaces of the outer strips, and bottom surface of the middle strip (Fig. 1). This minimises the transfer of shear forces from the RC beam to the masonry infill and thus enables unrestricted movement of the RC beam along the top of the masonry infill. The strips at the top and bottom of the masonry infill are thinner (15 mm thick) and they possess higher stiffness, which is important for providing sufficient stability to the masonry infill against out-of-plane loads, as explained in [44]. Through this strategic distribution of elastomeric strips with different stiffnesses, the decoupling system improves the seismic performance of infilled RC frames by delaying the masonry infill activation under in-plane loads, and at the same time providing stable boundary conditions against out-of-plane seismic loads. Moreover, the construction of decoupled masonry infills closely follows that of traditional masonry infills, with elastomeric strips as the only new on-site material, which is an additional advantage of the system. Detailed construction steps and material properties are provided in [44].

3. Finite element model and simulations of experimental tests

In this study, the numerical model originally developed by [15] is employed. This chapter summarises the main features of the model, while a more detailed description can be found in [15]. The Finite Element Package Abaqus [48] is used to generate the three-dimensional finite element model and for the subsequent execution of numerical simulations. As explained in [15], a simplified micro-modelling approach is applied in the study. This means that all elements of the infilled RC frame are modelled with proper finite elements, with the exception of mortar joints, which are modelled using zero-thickness contact definition. Therefore, the behaviour of mortar joints and their contacts to the bricks and frame is depicted by defining the contact definition.

3.1. Model geometry, mesh, boundary conditions and load application

Fig. 2 illustrates the numerical model of an experimentally tested RC frame with a solid decoupled masonry infill. The detailed dimensions of the experimental specimens are provided in [44], and the specimens are modelled with their actual dimensions to enable a direct comparison between experimental and numerical results.

To reduce computational time, the stiff RC bottom beam is replaced by three rigid plates: two tied to the RC columns and one beneath the masonry infill, allowing separate measurement of their reaction forces. This setup enables direct evaluation of column base shear, masonry infill

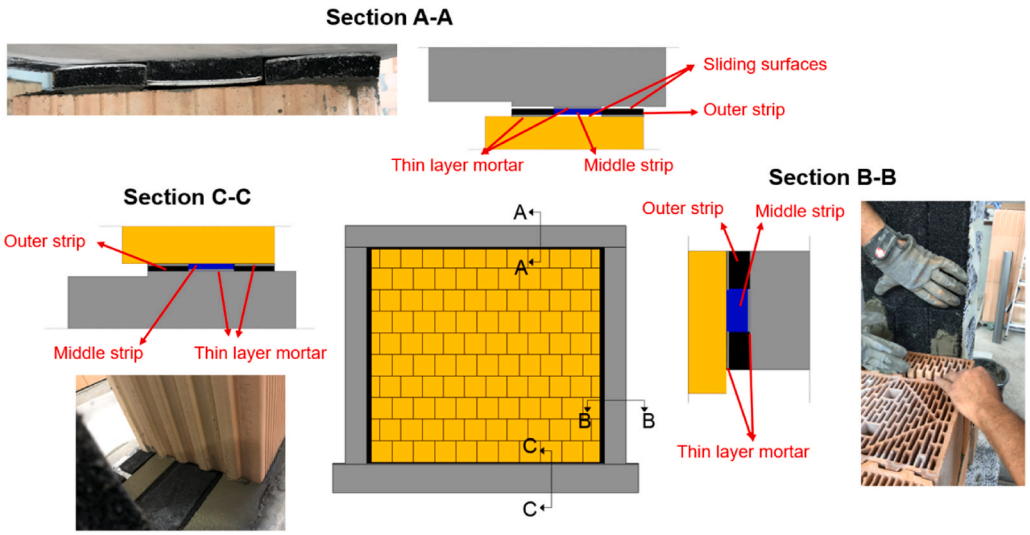

Fig. 1. RC frame with decoupled masonry infill.

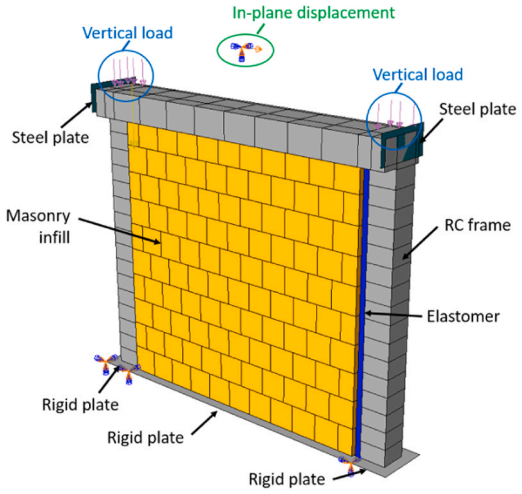

Fig. 2. RC frame with decoupled masonry infill with boundary conditions and all applied loads.

base shear (V_{INF}), and total infilled frame base shear (V_{IF}) as their sum.

Furthermore, to extract the internal forces in the post-processing of the results, seventeen cross-sections are defined along each RC column (Fig. 2). In the numerical model, each cross-section (surface) is defined as an „integrated output section“. Afterwards, corresponding „integrated variables“ (shear forces and bending moments) are requested for all „integrated output sections“ (cross-sections). In this way, the shear forces and bending moments integrated over the selected surfaces (cross-sections) are obtained and used to generate the diagrams on RC columns.

As in [15], three-dimensional eight-node hexahedral continuum elements with reduced integration (C3D8R) are selected to model concrete, masonry and elastomer units. The utilisation of these elements is recommended for explicit dynamic analysis [49], which is employed in this study. The reinforcement of the RC frame is modelled with two-dimensional truss elements (T3D2). Following [15], a global mesh size of 0.05 m is adopted for the frame and bricks, based on a sensitivity study confirming its suitability. A denser mesh is adopted only for elastomer strips due to their smaller dimensions. The mesh size is selected to provide three finite elements across the thickness of the elastomer.

As the experimental specimens are rigidly attached to a strong reaction floor, all translational and rotational degrees of freedom of the bottom rigid plates are restrained. The fixation of the lower beam is the only boundary condition in the experimental campaign [44]. However, in order to apply in-plane displacements to the frame in the numerical model, steel plates are positioned at the outer edges of the upper beam. The predetermined in-plane displacements are applied to the steel plates. In this way, the in-plane loads are applied displacement-controlled, as in the corresponding experimental tests [44].

In addition to the initial loading step, in which the boundary conditions are defined, a total of three individual loading steps are required to simulate the load application in the experimental tests: 1) Gravity time step, in which the dead load of the construction is applied, 2) Vertical load step, in which the total vertical force of 200 kN per column is applied, as in the experimental tests, and 3) in-plane loading step, in which the infilled frame is monotonically loaded up to the desired in-plane displacement (drift), from left to right.

In-plane loading is applied monotonically instead of cyclically to avoid unnecessary model complexity, as it has limited impact on the main objectives of the study, which are examining deformation mechanisms, force distribution, and decoupling efficiency. This assumption is also justified because the decoupling prevents cyclic damage from occurring in the masonry infill. Moreover, [50] reported that monotonic loading yields only about 10 % higher strength than cyclic loading, justifying its use here.

3.2. *Definition of materials and interactions*

The concrete damage plasticity (CDP) model available in [48] is used to model the behaviour of concrete and masonry, which are both considered quasi-brittle materials. The CDP model allows a separate definition of the material response under compressive and tensile stresses.

Since the same frame as in [15] is used, the concrete material parameters are taken from [15], where the concrete modelling approach is thoroughly described and material parameters are calibrated using a bare frame experimental test. Reinforcing steel is modelled as an elasto-plastic material. Its elastic behaviour is characterised by the modulus of elasticity and Poisson’s ratio, while the plastic behaviour is defined by the yield stress (f_y) and ultimate stress (f_u). The input data required for the material definition of steel reinforcement are shown in Table 1.

Table 1
Material properties for the reinforcement steel.

Unit	D [mm]		
	10	12	14
E_{r0} [GPa]	200	195	200
ν [-]	0.3	0.3	0.3
f_y [MPa]	500	510.75	461.2
f_u [MPa]	540	805.5	695.5
ε_u [%]	5	7.88	10.13

The CDP model is used as a constitutive model for masonry. The behaviour of masonry is simulated as in the study of [15], according to the recommendations of [21]. Namely, masonry units obtain the material characteristics of the masonry assembly. The stress-strain curves are generated following the equation of [21] too, but with a slightly different softening branch in compression, as proposed by [15]. As for concrete, the elastic behaviour of masonry is linear and isotropic. The modulus of elasticity is determined experimentally [44], while Poisson's ratio is adopted as $\nu = 0.19$. The inelastic behaviour is defined separately for compression and tension, which will be described in the following. The plasticity parameters for masonry are adopted as in the original model of [15].

As some parameters were not measured experimentally, additional recommendations from the literature are adopted to form the material curves. Due to this, the material curves for masonry are discussed in more detail in this chapter. Fig. 3 shows the stress-strain curve of masonry in compression. The response in compression is linear between points A and B. The stress at point B is determined according to the proposal of [51], as $\sigma_B = 0.33\, f_m$. The inelastic part of the curve between points B and D is defined by the equation proposed by [21]:

$$\sigma(\varepsilon) = f_m\left(2\frac{\varepsilon}{\varepsilon_1} - \frac{\varepsilon^2}{\varepsilon_1^2}\right) \tag{1}$$

Herein, f_m is the masonry compressive strength, experimentally determined in [44], and ε_1 is the corresponding strain, which is calculated following the equation proposed by [51]:

$$\varepsilon_1 = C_j \frac{f_m}{E_m^{0.7}} \tag{2}$$

$$C_j = \frac{0.27}{f_j^{0.25}} \tag{3}$$

In Eq. (2) E_m is the modulus of elasticity of masonry, and Cj is a factor that depends on the compressive strength of mortar f_j, determined in [44], and it is calculated according to Eq. (3).

The final descending section of the curve, after point D, is defined using the equation proposed by [15]:

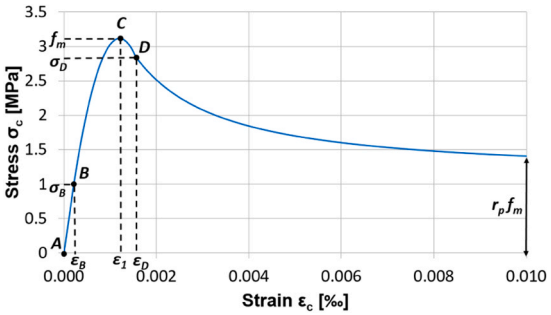

Fig. 3. Stress-strain curve of masonry in compression.

$$\sigma = \sigma_D + \left\{\left[\sin\left(1 - e^{\left[\frac{f_m}{E\cdot\varepsilon}\left(\frac{\varepsilon}{\varepsilon_1} - \frac{\varepsilon_D}{\varepsilon_1}\right)\right]}\right)\right]\pi\cdot\alpha\right\} \tag{4}$$

Where σ_D is calculated as $\sigma_D = 0.9\, f_m$, as suggested by [51]. The coefficient α controls the residual strength of masonry, and it is calibrated to achieve a close agreement with the experimental result of test T2 on the traditional masonry infill specimen, reported in [52].

The stress-strain curve for masonry in tension is defined according to the following equation proposed by [21]:

$$\sigma(\varepsilon) = f_{mt}\left[r_t + (1 - r_t)e^{\left(\frac{-\alpha_1(\varepsilon - \varepsilon_{cr})}{f_{mt}}\right)}\right] \tag{5}$$

Herein, f_{mt} is the masonry tensile strength, and ε_{cr} is the corresponding strain. The parameters r_t and α_1, defining the descending branch of the curve, are calibrated using the experimental result of test T2 [52]. As recommended by [21], tension is defined using displacement (crack width) instead of strain. In order to calculate the displacement (crack opening) from the strain, the following formulation proposed by [53] is used:

$$\varepsilon = \varepsilon_{cr} + \frac{u}{l_{eq}} \tag{6}$$

Where l_{eq} is the length of the used finite element.

The damage variables in compression and tension (d_c, d_t), which account for the degradation of the elastic stiffness, are calculated according to [54]:

$$d_c = 1 - e^{-a_c \varepsilon^{in}} \tag{7}$$

$$d_t = 1 - e^{-a_t \varepsilon^{in}} \tag{8}$$

Where ε^{in} denotes the inelastic strain, and a_c and a_t are parameters for the uniaxial compression and tension, respectively, which are calibrated to match the experimental response of test T2 [52].

Table 2 summarises the masonry material input data.

In experimental tests, the decoupling of masonry infills from RC frames is achieved by installing three strips made of elastomeric material, as described in Chapter 2. Because of its hyperelastic behaviour, the elastomeric material in the numerical model is modelled using a suitable hyperfoam material model already available in [48]. The material definition in [48] allows using the experimental stress-strain curves for both elastomeric mixtures (Elastomer 1 and Elastomer 2). Since the elastomer strips are subjected to compressive and shear stresses when

Table 2
Masonry material input data.

Unit	Value	Source
E_m [GPa]	4.7	Experiment
f_m [MPa]	3.1	Experiment
$\varepsilon_{m,el}$ [‰]	0.22	[51]
ε_1 [-]	1.2	[51]
σ_D [MPa]	2.81	[51]
ε_2 [-]	1.6	[15]
α [-]	0.8	Calibrated
a_c [-]	240	Calibrated
f_{mt} [MPa]	0.22	Calculated
ε_{cr} [-]	0.0464	Calculated
r_t [-]	0.06	Calibrated
α_1 [-]	200	Calibrated
a_t [-]	280	Calibrated
l_{eq} [m]	0.05	[15]
ν [-]	0.19	[15]
f_j [MPa]	12.8	Experiment
f_b [MPa]	11.0	Experiment

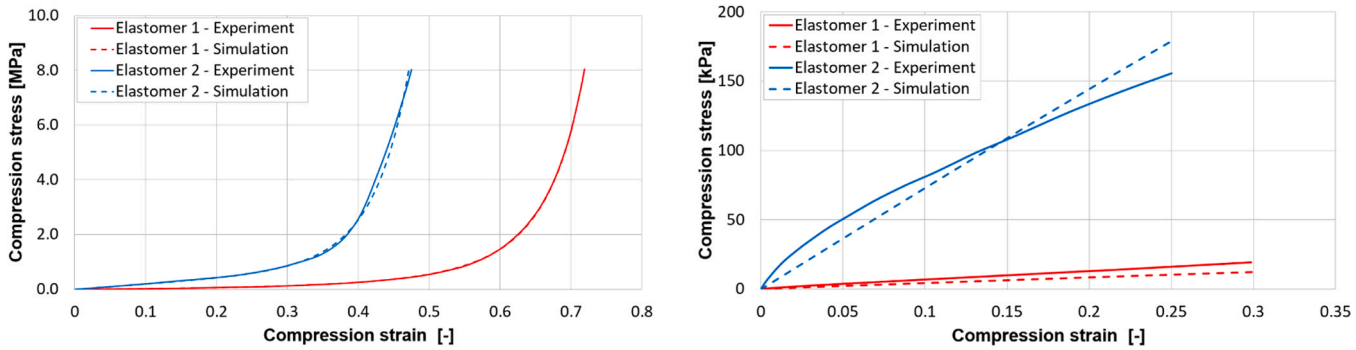

(a) (b)

Fig. 4. Experimental and numerical stress-strain curves of Elastomer 1 and Elastomer 2 material under: compression (a) and shear (b).

the masonry infills are loaded with in-plane and out-of-plane loads, the experimental data from the corresponding compression and shear tests is used. The only value that needs to be calibrated in the material model is the strain energy potential order, which is set to 2, as in [15]. Fig. 4 shows a good match between experimental and numerical stress-strain curves of both elastomer mixtures for both compression and shear. The influence of cyclic loading on the elastomer can be neglected, as it shows nearly identical monotonic and cyclic responses [44] and fully recovers its shape after unloading, confirmed by tests in [44] and [55].

As the numerical model is composed of many individual elements, such as RC frame members, brick units and elastomeric profiles, it is necessary to properly define the interactions between these different parts of the model. In order to achieve this, the same approach to modelling of interactions is applied as in [15]. Namely, the general contact available in [48] is used with different interaction properties. In total, four individual contact properties are defined. The first one is the general interaction property that includes the definition of normal and tangential behaviour. The normal behaviour is defined as "hard" contact, and tangential behaviour is determined by defining a friction coefficient. The value of the friction coefficient is set to 0.6, based on recommendations of a previous study [15]. The general interaction property is automatically assigned to all contacts and is subsequently overwritten if other interaction properties are applied to a specific contact. The second two interaction properties are related to modelling mortar joints. For all mortar connections, it is necessary to define cohesive behaviour and damage evolution in addition to the definition of normal and tangential behaviour. The linear elastic part of the cohesive behaviour is defined by normal (k_{nn}) and shear stiffnesses (k_{ss} and k_{tt}), which are calculated according to [56]:

$$k_{nn} = \frac{E_u \cdot E_m}{E_u(h_u + t_j) - E_m \cdot h_u} \tag{9}$$

$$k_{ss} = k_{tt} = \frac{k_{nn}}{2(1+\nu)} \tag{10}$$

In Eqs. (9) and (10), E_u and E_m are the modulus of elasticity of the brick unit and masonry, respectively, and h_u is the brick height, and t_j is the joint thickness. The modulus of elasticity of brick is equal to approximately $500f_b$, as recommended in [51].

As in [15], the damage initiation criterion is chosen to be a quadratic traction, and it is a function of the maximum tensile (t_n^0) and shear stresses (t_t^0 and t_s^0), while the energy-based exponential mixed-mode evolution power law [57] is selected to determine the damage evolution. This power law is a function of the fracture energies in the normal (G_n) and shear directions (G_s, G_t) and a cohesive property parameter η. Further details on the modelling of the interactions with more detailed theoretical background can be found in [15]. Table 3 summarises parameters required to define the mortar joints behaviour. The values of maximum shear stresses (t_t^0 and t_s^0) are determined experimentally [58].

Table 3
Interaction properties.

Unit	Value	Source
k_{nn} [GPa/m]	269.5	[56]
k_{ss} [GPa/m]	11.3	[56]
k_{tt} [GPa/m]	11.3	[56]
t_n^0 [MPa]	0.2	[15]
t_t^0 [MPa]	0.2	Experiment
t_s^0 [MPa]	0.2	Experiment
G_n [N/m]	20	[15]
G_s [N/m]	20	[15]
G_t [N/m]	20	[15]
η [-]	2	[15]
μ [-]	0.7	[15]

The remaining parameters, such as t_n^0, G_n and G_s and μ are assigned values similar to those used in the previous study [15].The last interaction property is used to model the effect of the sliding surfaces, which are placed between the top surfaces of the elastomer strips and concrete / masonry. As for other interactions, the normal behaviour is defined as "hard", while for the tangential behaviour, a low friction coefficient, equal to 0.1, as provided by the producer [44] is employed.

3.3. Simulations of the in-plane tests on decoupled infilled RC frames

The numerical model is used to simulate the in-plane loading phases of the sequential loading tests on RC frames with decoupled masonry infills: without opening (test D2), with window (test D5) and with door opening (test D8). In Table 4, numerical force-drift curves are compared with the positive and negative branches of the experimental force-drift envelopes. All specimens are simulated using the same set of input parameters discussed in Chapter 3.2, without case-specific adjustments to reach a "perfect" fit for all cases. The comparison shows a reasonably good match between experimental and numerical results in terms of initial stiffness, maximum horizontal load, and stiffness degradation, for all configurations. The deviation at higher in-plane drift levels for specimen D5 results from faster damage accumulation in the numerical model. However, this deviation is conservative and does not affect the development of the design concept, as FprEN 1998–1–2:2025 [45] limits the maximum in-plane drift in the SD limit state to 2.0 %. However, when extending the model to other masonry types or mortar joints, calibration and validation through experimental tests at different scales are required.

4. Parametric study

The numerical model is used to investigate the in-plane response of infilled RC frames with different opening arrangements in the decoupled masonry infills. The cases of solid masonry infill, masonry infills with

Table 4
Comparison of experimental and numerical force-drift curves of decoupled infilled RC frames.

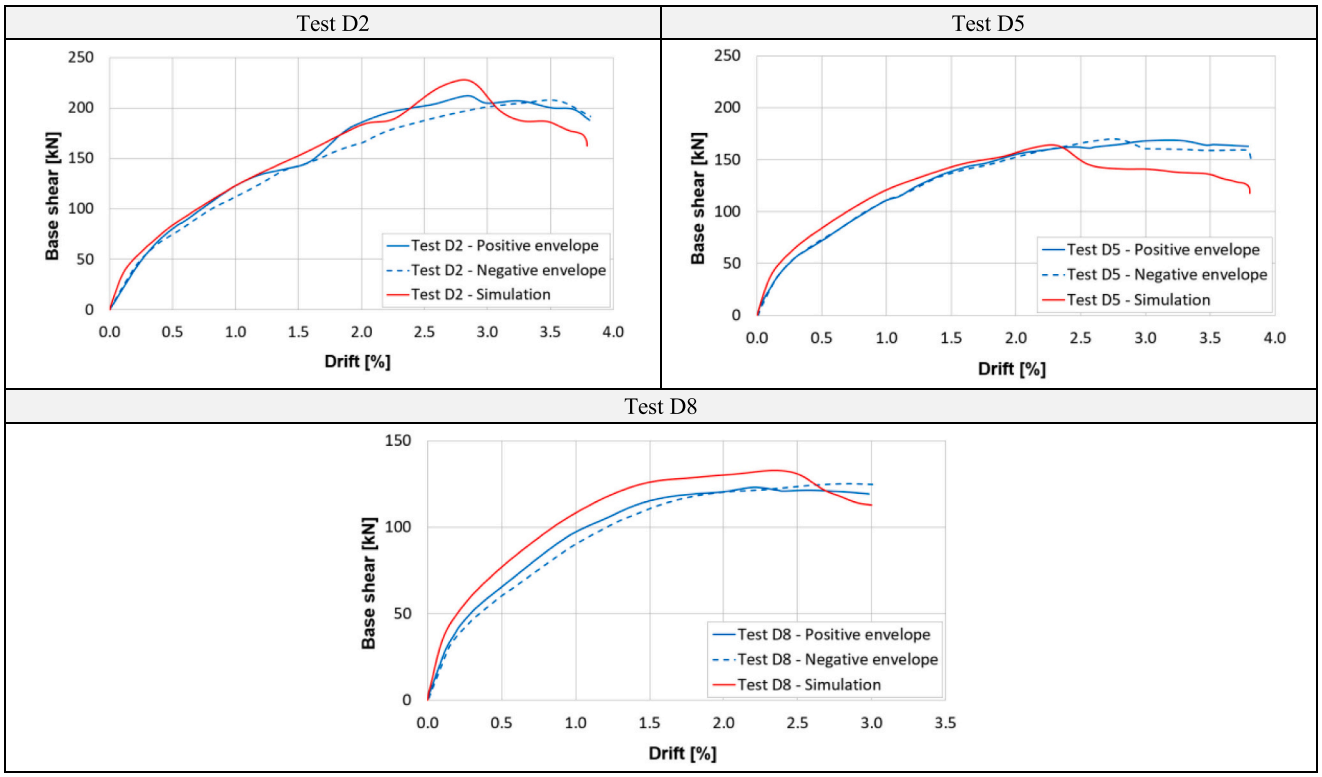

windows, and full-height door openings, each with different dimensions and locations within the masonry infill, are considered. In addition to this, the case of a partially infilled frame is investigated. The influence of vertical load is not investigated, as [15] showed it only slightly increases initial stiffness but has negligible effect on overall in-plane behavior.

In the model name (simulation), the major characteristics of the investigated masonry infills are summarised. The first letter indicates the type of opening: W for a window, D for a door, and PI for a partial masonry infill. The second part specifies the location of the opening: C (centric), TL (top-left), TR (top-right), L (left side) and R (right side). Numbers (20, 30, 40 or 50) denote the percentage of the opening relative to the panel. For example, W-C20-D refers to an RC frame with a decoupled masonry infill with a centric window opening covering approximately 20 % of the panel. Furthermore, all simulations of RC frames with decoupled masonry infills are carried out for the experimentally tested decoupling system with a 50 mm thick vertical, and 15 mm thick horizontal elastomeric strips, whose stress-strain relationships are presented in Fig. 4. In all simulations in Chapters 4.1–4.4, sliding profiles are placed only at the top with a friction coefficient of 0.1, as in the experimental campaign [44]. In the additional simulations (Chapter 4.5), the same friction coefficient is applied at both the top and bottom.

4.1. *Solid masonry infill*

The decoupled infilled frame without openings, also experimentally tested in test D2, is analysed first. Fig. 5a compares the force-drift response of the decoupled infilled frame and that of the bare frame. Due to the decoupling system, the initial in-plane stiffness of the decoupled infilled frame is equal to that of the bare frame. In addition,

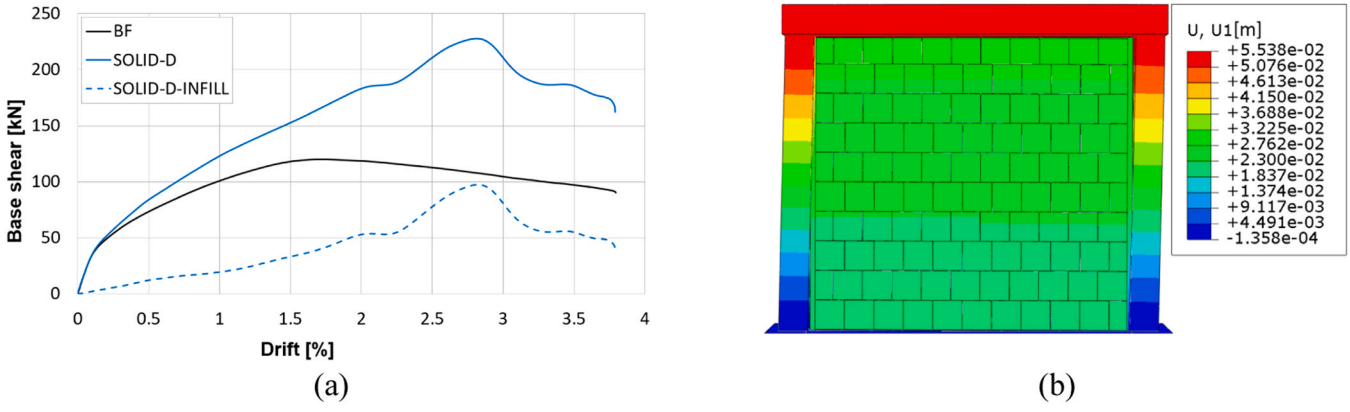

Fig. 5. Force-drift curves of the bare frame, decoupled infilled frame and decoupled masonry infill (a) and horizontal displacements plot on decoupled fully infilled frame at 2.0 % of in-plane drift (b).

Fig. 5b presents horizontal displacements of both the frame and the masonry infill at an in-plane drift of 2.0 % (corresponding to 55 mm of frame in-plane displacement). The horizontal displacements plot indicates that the frame deformation is absorbed by the compression of the elastomeric strips at the sides (top-left and bottom-right corners), in combination with sliding mechanisms at the top and bottom of the masonry infill. Sliding is more pronounced at the top, where dedicated sliding surfaces are present. However, it is activated at the bottom too, despite the absence of such surfaces, which enables compression of the elastomeric strips at the bottom-right corner too.

As a result of the decoupling effect, the base shear force of the masonry infill increases slowly and gradually, leading to only minor deviations between the force-drift responses of the decoupled infilled frame and the bare frame, particularly up to 2.0 % of in-plane drift (Fig. 5a). At around 2.0 % of in-plane drift, the initial stepwise cracking in the masonry infill emerges, resulting from the bed joint cracking and the opening of unmortared head joints. This cracking mechanism activates multiple diagonal compression struts within the masonry infill, as observed in experimental test D2, and produces a more pronounced increase in the base shear force of both the infilled frame and masonry infill (Fig. 5a).

Furthermore, Table 5 indicates that the shear forces at the loaded corners of the decoupled infilled frame (top-left and bottom-right) begin to increase gradually for in-plane drifts larger than 0.5 %. The bending moment distribution remains nearly unchanged relative to the reference bare frame, with the first notable variation occurring at 2.0 % of in-plane drift, where a null point in the bending moment diagram shifts slightly upward. Overall, the results demonstrate that the masonry infill has almost no influence on the RC frame response up to the maximum design in-plane drift of 2.0 %. Because of the delayed masonry infill activation, the decoupled masonry infill attains significant damage (SD) limit state condition defined by [59] at 3.0 % of in-plane drift (Fig. 6).

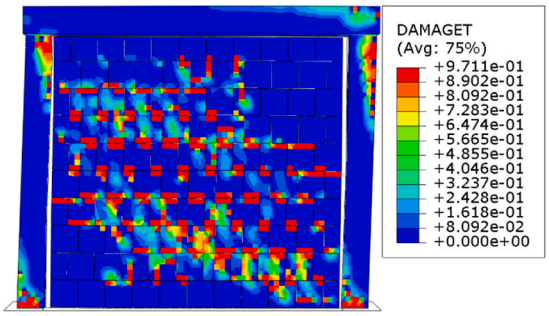

Fig. 6. Specimen SOLID-D: Damage pattern at SD limit state at 3.0 % of in-plane drift.

4.2. *Masonry infills with window openings*

The in-plane behaviour of RC frames with decoupled masonry infills containing centric window openings is governed by a specific load-resisting mechanism. For example, in configuration W-C20-D – also experimentally tested as specimen D5 – numerical simulation shows that up to 2.0 % of in-plane drift, the only damage to the masonry infills consists of light cracking around the window corners. This localised and controlled damage, also observed experimentally in [44], occurs at low in-plane drift levels and enables the separate rotation of two infill piers. This leads to the generation of two steep diagonal struts in each infill pier, which are activated only at high in-plane drifts ($\Delta > 2.0$ %), after the full compression of the elastomers in the strut corners (Fig. 8a). The development of this mechanism allows absorption of the frame deformation and reaching high in-plane drifts with low level of masonry infill activation and damage. For specimen W-C20-D, the significant damage (SD) limit state is reached at 2.7 % of in-plane drift (Fig. 8b), and for other decoupled masonry infills with the centric window opening at

Table 5
Comparison of internal forces on the bare RC frame and RC frame with solid decoupled masonry infill.

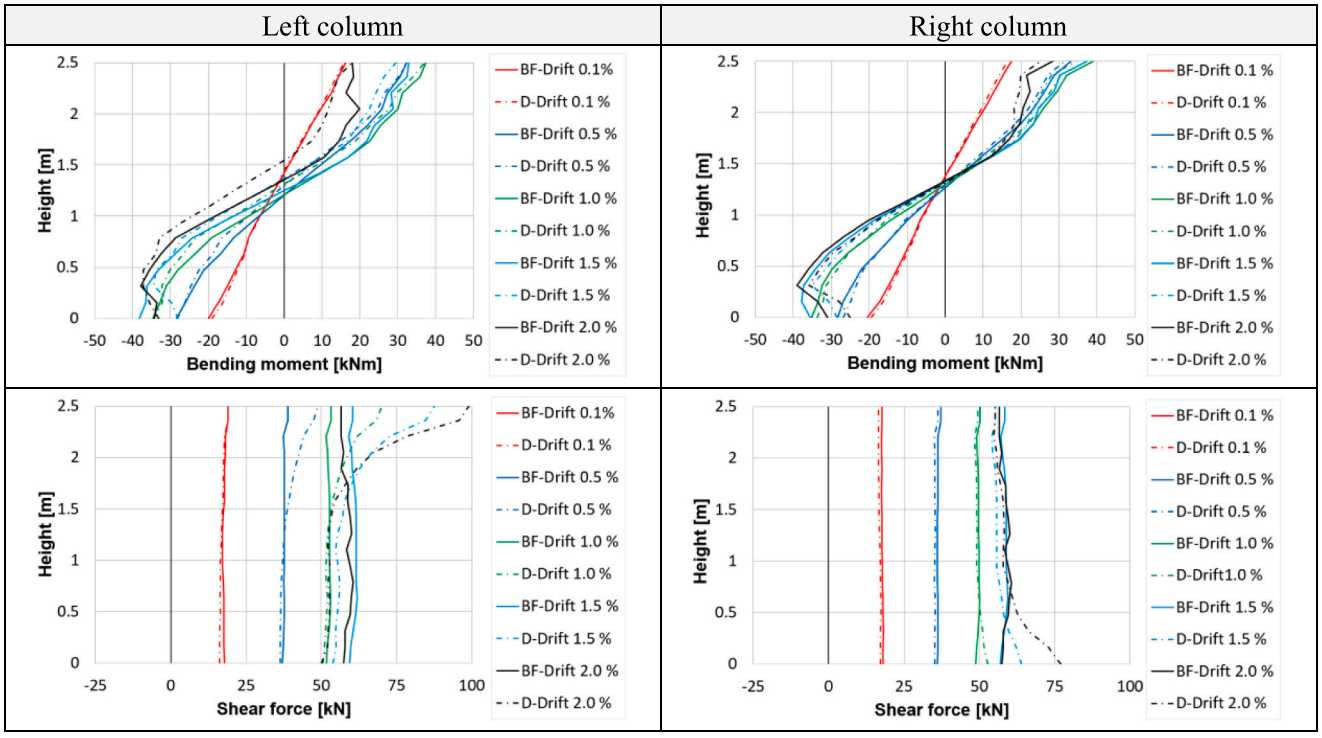

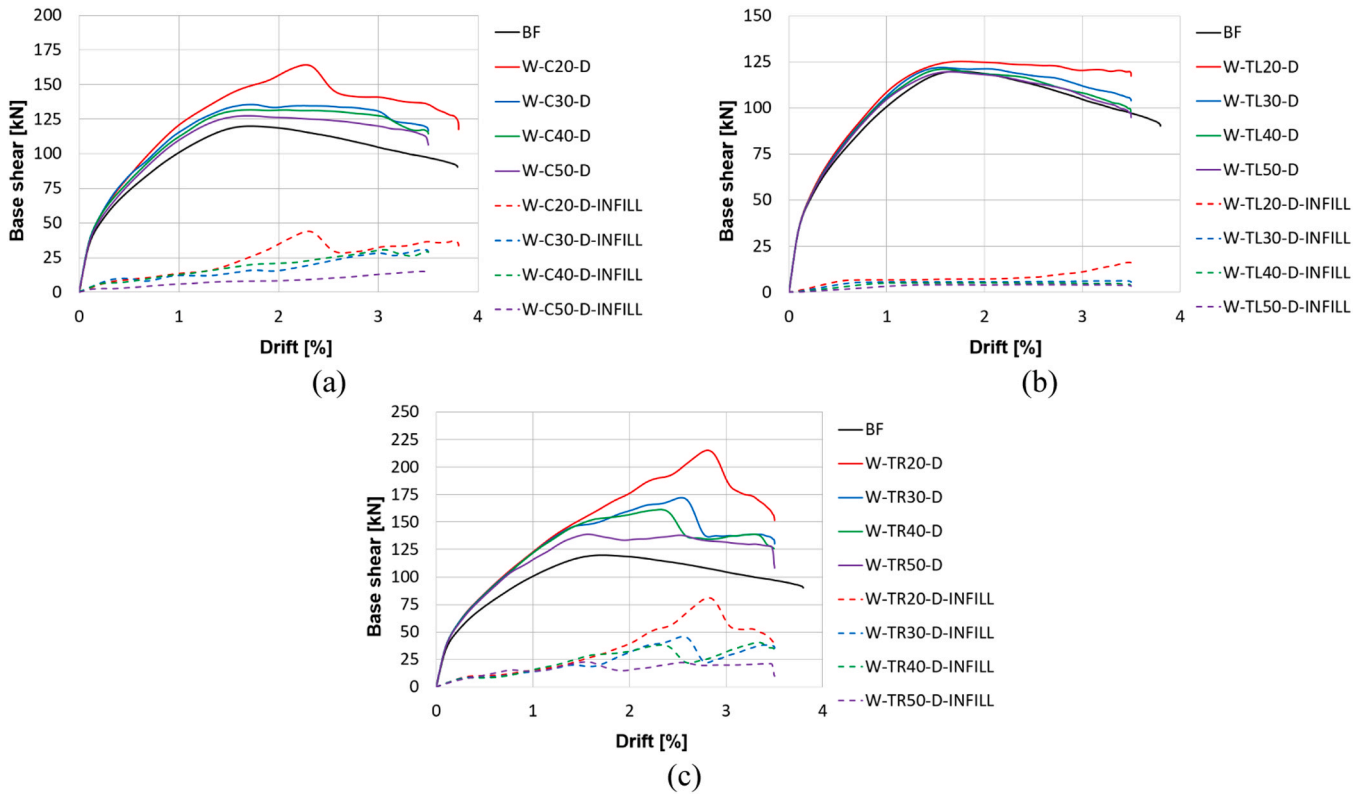

Fig. 7. Force-drift curves of decoupled infilled RC frames and decoupled masonry infills with window openings located at the infill centre (a), top-left (b) and top-right corner (c).

Table 6
Distribution of shear forces on the RC frame with decoupled masonry infill with a 20 % centric window opening (W-C20-D).

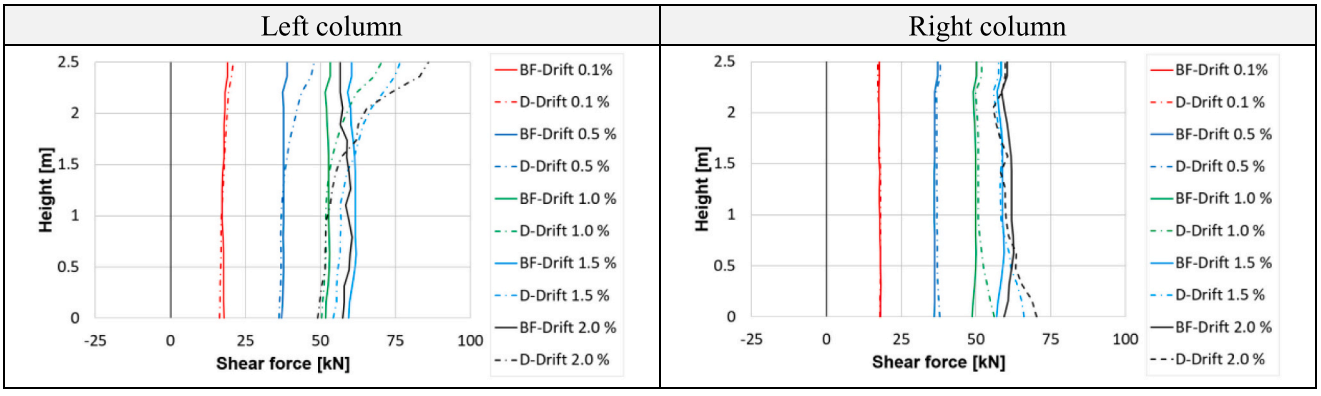

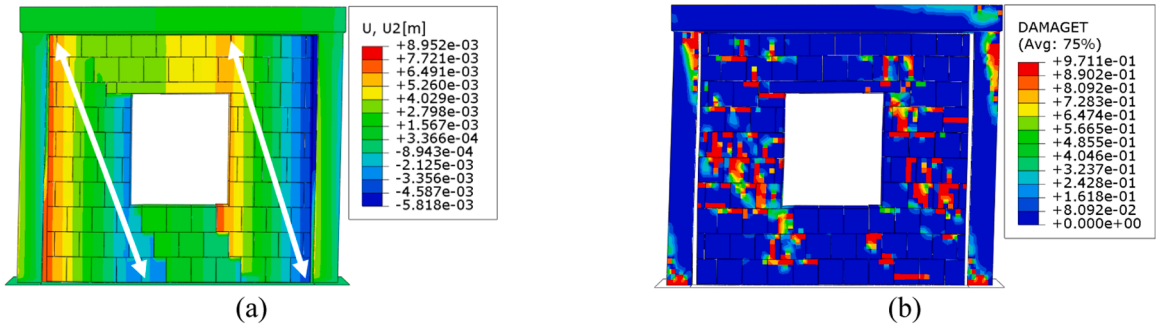

Fig. 8. Numerical simulation W-C20-D: Vertical displacements plot at 2.0 % of in-plane drift (a) and damage pattern at SD limit state at 2.7 % of in-plane drift (b).

in-plane drifts between 2.5 % and 3.0 %. Furthermore, Fig. 7a shows that the force-drift response of the decoupled infilled frames with centric window openings closely resembles that of the bare frame, with rather small base shear forces reached by masonry infills across all openings sizes. Table 6 indicates a small and controlled increase of the shear forces on the frame, at in-plane drifts larger than 0.5 %, slightly more at the top of the left than at the bottom of the right column, due to the generated diagonal strut actions in the infill piers. The distribution of shear forces is shown only for the RC frame with the decoupled masonry infill with a centric window opening of 20 %, as for higher opening percentages the interaction effects are even less pronounced. The column bending moments remain nearly identical to those of the reference bare RC frame and are therefore not presented herein.

The results show that decoupled masonry infills with centric window openings develop an alternative mechanism to accommodate frame deformation compared with solid decoupled masonry infill. However, this mechanism also effectively delays the activation of the masonry infill, allowing the surrounding RC frame to deform and behave like a bare frame (Fig. 8b).

For window openings located at the top-left (loaded) corner, the transfer of shear forces is minimised because contact between the masonry infill and the frame occurs only in the central area, where frame deformations are smaller and the compression strut forms at a shallower angle. In addition, force transfer is reduced by the sliding along the top interface, compression of the soft elastomeric profiles adjacent to columns and sliding effects at the bottom (Fig. 9a). As a result of this behaviour, almost no difference between the force-drift curves of bare and decoupled infilled frames can be seen (Fig. 7b). The base shear force of the masonry infill is almost negligible (Fig. 7b), and masonry infills remain undamaged in all models up to the ultimate in-plane drift of 3.5 %. Table 7 shows that only at in-plane drifts larger than 0.5 %, a slight increase of the shear force can be noticed at the upper parts of the left column. Since there is almost no change in the distribution of bending moments in comparison with the bare RC frame, the bending moment diagrams are not presented.

As shown in Fig. 7, masonry infills with top-right (non-loaded) window openings (W-TR) show slightly greater deviation from the bare frame and higher masonry infill activation than other window configurations (W-C, W-TL). For the smallest opening (W-TR20-D), the compression strut in the masonry infill can form similarly to that in a fully infilled frame (SOLID-D), resulting in nearly identical in-plane force-drift curves for these configurations. The compression strut is only slightly more shallowly inclined (Fig. 9b).

With increasing opening size (specimens W-TR30-D, W-TR40-D, W-TR50-D), the compression strut in the masonry infills becomes steeper (Fig. 10a,b), and part of the masonry infill next to the loaded (left) column performs rotation (Fig. 10a,b), while part of the masonry infill below the opening undergoes sliding (Fig. 10a,b). This mechanism causes minor cracking near the opening corner at low in-plane drifts but delays further damage, allowing the masonry infill to accommodate frame deformations effectively up to in-plane drifts beyond 2.0 %. Depending on the opening size, the significant damage (SD) limit state is reached between 2.3 % and 3.0 % of in-plane drift.

Among all opening sizes, the W-TR20-D specimen shows the strongest frame-infill interaction, limited to a moderate increase in column shear near the loaded corners from 0.5 % of in-plane drift onward (Table 8). Larger openings cause even smaller shear demands.

4.3. Masonry infills with door openings

Fig. 11a presents the force-drift curves from simulations on RC frames with decoupled masonry infills containing door openings of various sizes and locations. For configurations with centric door openings, high in-plane drifts are achieved without masonry infill damage because of the rotation of the left infill pier and sliding of the RC beam against the right infill pier, which remains inactive throughout the simulation (Fig. 11b). This behaviour has also been observed in experimental test D8. As a result, masonry infill activation is negligible, and only a minimal discrepancy is observed between the force-drift responses of the infilled and bare frames (Fig. 11a). Additionally, the internal force distribution remains unchanged compared to the bare RC frame. The decoupled masonry infill in model D-C40-D reaches the significant damage (SD) limit state at an in-plane drift of 2.89 % (Fig. 12a), while in the model D-C50-D, this occurs at an even higher in-plane drift of 3.4 %.

If the door opening is located next to the left column, the force-drift curves indicate a complete absence of masonry infill activation, and the RC frames with the decoupled masonry infills behave identically to the reference bare RC frame (Fig. 11a). This response results from the full-height door opening on the loaded side and the unhindered sliding of the top beam along the right infill pier. As the masonry infills remain completely inactive, they sustain no damage up to the ultimate in-plane drift of 3.5 % and have no influence on the distribution of internal forces on the RC columns.

In the case where the door opening is located on the right side of the masonry infill, the RC frames with decoupled masonry infills also exhibit behaviour closely resembling that of the bare RC frame. As shown in Fig. 11a, the initial in-plane stiffnesses of the bare frame and the infilled frames are identical. With increasing in-plane drift, a slight divergence in the force-drift curves and a small increase in base shear force of the masonry infill can be observed (Fig. 11a), although these effects remain insignificant. Furthermore, Fig. 12b shows a slight increase in shear force measured at the loaded corner of the left column, at in-plane drifts larger than 0.5 %, while the bending moment distribution remains unchanged from that of the reference bare frame and is therefore not presented. The results in Fig. 12b correspond to the configuration with a 40 % opening. For the model with a larger opening (50 %), interaction effects are even less significant and are not presented. The significant damage (SD) to decoupled masonry infills in models D-R40-D and D-R50-D appears at around 3.2 % and 2.4 % of in-plane drift, respectively. However, damage patterns are not additionally presented as they are similar to those already presented in Fig. 12a, for the left infill pier.

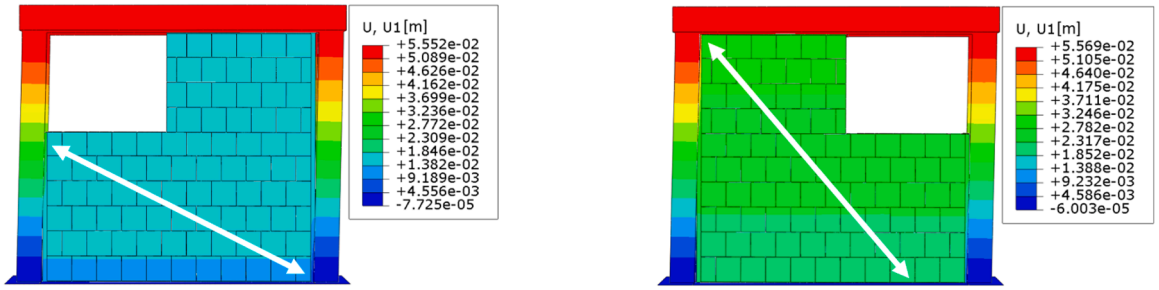

Fig. 9. Horizontal displacements at 2.0 % of in-plane drift: Specimen W-TL20-D (a) and W-TR20-D (b).

Table 7
Distribution of shear forces on the RC frame with decoupled masonry infill with a 20 % of window opening located at the top-left corner (W-TL20-D).

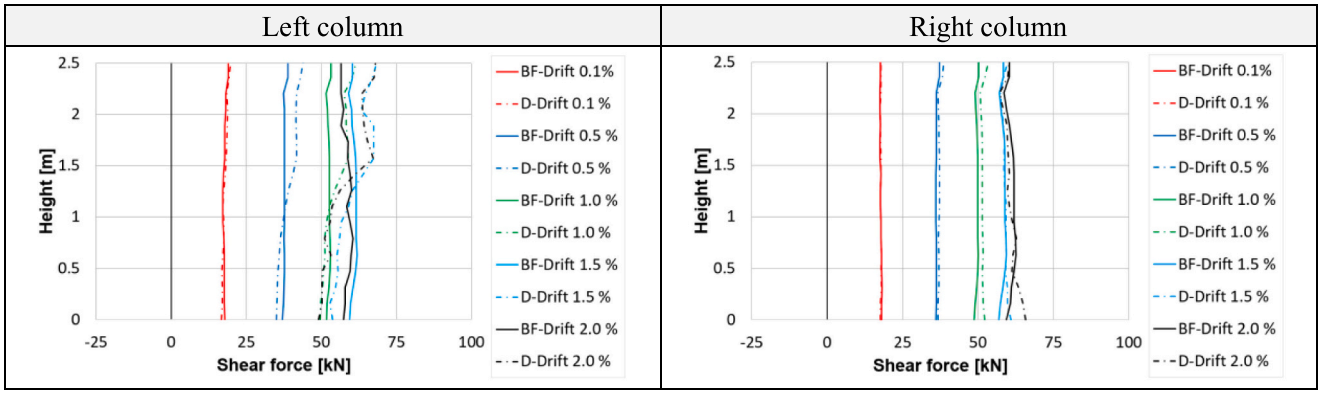

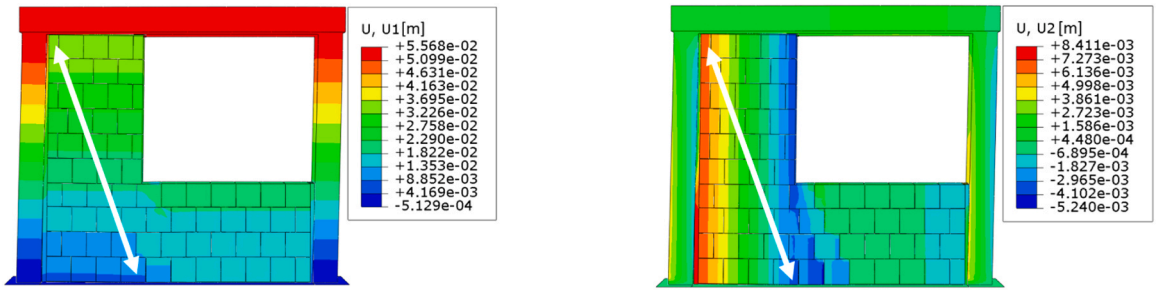

Fig. 10. Numerical simulation W-TR40-D: Horizontal displacements (a) and vertical displacements plot (b) at 2.0 % of in-plane drift.

Table 8
Distribution of shear forces on the RC frame with decoupled masonry infill with a 20 % of window opening at the top-right corner (W-TR20-D).

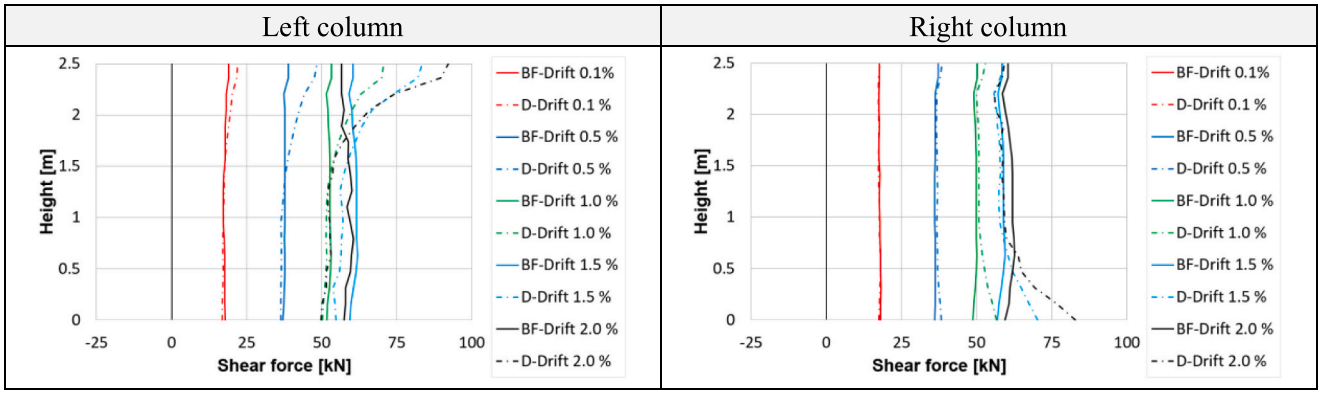

4.4. *Partially infilled frames*

Partially infilled RC frames with total opening percentages of 30 % and 50 % are also investigated. In these configurations, combined compression of vertical elastomeric profiles and sliding at the bottom absorb column deformation and prevent masonry infill activation, as shown at 3.5 % of in-plane drift for the PI-30-D configuration (Fig. 13b). Consequently, masonry infills remain almost entirely unactived, and the force-drift response of the decoupled partially infilled frames closely matches that of the bare frame (Fig. 13a).

In addition, only a small increase of the shear forces at the top-left and bottom-right frame corner can be noticed. Results are shown only for the shear force distribution for the decoupled masonry infill with 30 % of opening (Table 9), as for the larger 50 % opening, the interaction is even smaller. The decoupling measures completely prevent damage to these masonry infills.

4.5. *Sliding interfaces at the top and bottom of the masonry infill*

Although frame–infill interaction is minimal across all configurations (Chapters 4.1–4.4), additional analyses are performed for the most activated cases within specimen groups (SOLID-D, W-TR20-D, D-R40-D) to evaluate whether adding sliding surfaces at the bottom of the masonry infill further reduces interaction. Supplementary simulations with equal friction at both interfaces ($\mu = 0.1$) are conducted, denoted as SOLID-DS, W-TR20-DS, and D-R40-DS.

The force–drift curves in Fig. 14 show that adding sliding surfaces at the bottom interface further improves decoupling. The maximum base

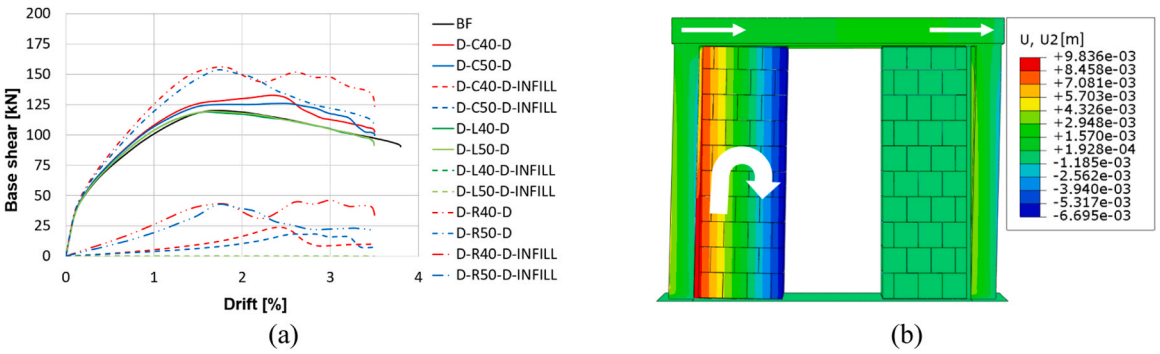

Fig. 11. RC frames with decoupled masonry infills with door openings: Force-drift curves of infilled decoupled frames and decoupled masonry infills (a); Numerical simulation D-C40-D: Vertical displacements plot at 2.0 % of in-plane drift (b).

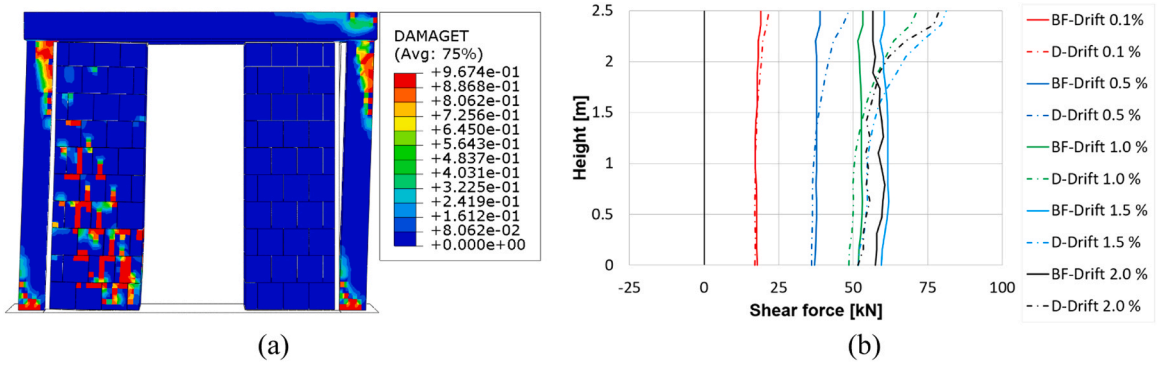

Fig. 12. Numerical simulation D-C40-D: Damage pattern at 2.9 % of in-plane drift (a) and distribution of shear forces on the left column of model D-R40-D (b).

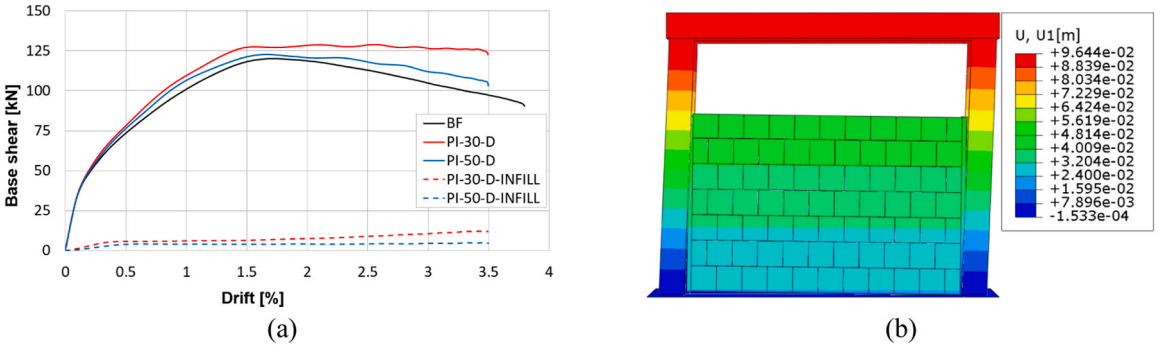

Fig. 13. Force-drift curves of the decoupled partially infilled RC frames and decoupled masonry infills (a) and horizontal displacements plot of the model PI-30-D at 3.5 % of in-plane drift (b).

shear forces of masonry infills are reduced by a factor greater than 4 in all variants. For SOLID-DS and W-TR20-DS, minor masonry infill activation occurs only beyond 2.4 % of in-plane drift, while D-R40-DS remains fully decoupled up to the ultimate in-plane drift.

The significantly higher decoupling efficiency is due to the full activation of the vertical elastomeric strips on both sides, allowing the system to accommodate twice the frame deformation. This is illustrated in Fig. 15 for the fully infilled RC frame SOLID-DS at an in-plane drift of 2.0 %. Sliding at the bottom interface activates both sides of the vertical elastomeric strips, resulting in deformations on each side of about half the elastomer thickness. A similar behaviour is observed for specimen W-TR20-DS.

5. Evaluation of the results of the parametric study

The following chapter analyses the results of the parametric study on decoupled infilled RC frames with regard to the achieved in-plane drift capacities and interaction effects. The findings from these analyses serve as the basis for developing a design concept presented in Chapter 6.2.

5.1. In-plane drift capacities

The decoupling system INODIS ensures that both solid and masonry infills with openings of various types, sizes, and locations remain largely unactivated up to an in-plane drift of 2.0 %. The frame deformation is primarily accommodated by compression of the side elastomeric strips and sliding mechanism at the top, if sliding interfaces are applied only at the top of the masonry infill. When sliding interfaces are provided at both the top and bottom, masonry infill activation is further minimised, and the elastomeric strips are engaged on both sides.

Across all opening configurations, the masonry infills exhibit distinct deformation mechanisms, but interaction between the RC frame and the masonry infills remains minimal. This confirms efficient decoupling and controllable behaviour even beyond 2.0 % of in-plane drift. Owing to

Table 9
Distribution of shear forces on columns of the decoupled partially infilled RC frame (PI30-D).

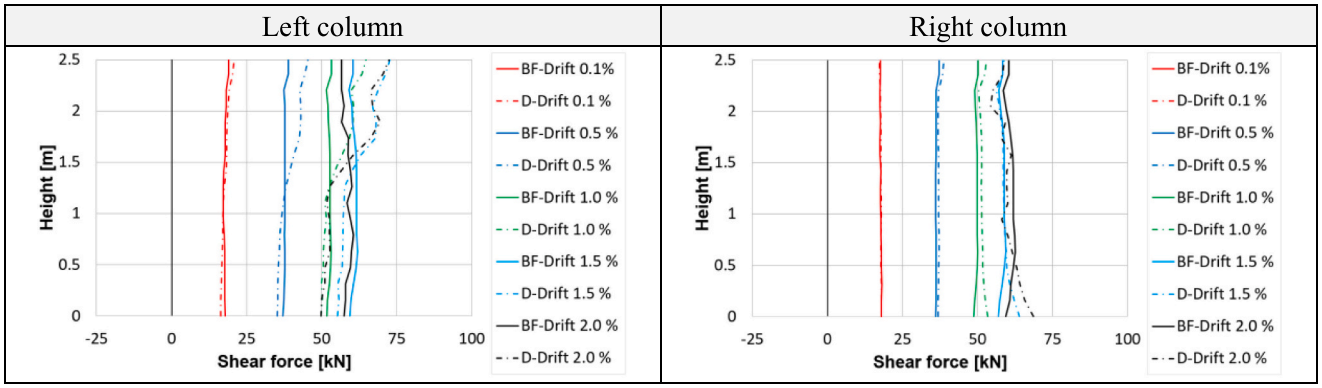

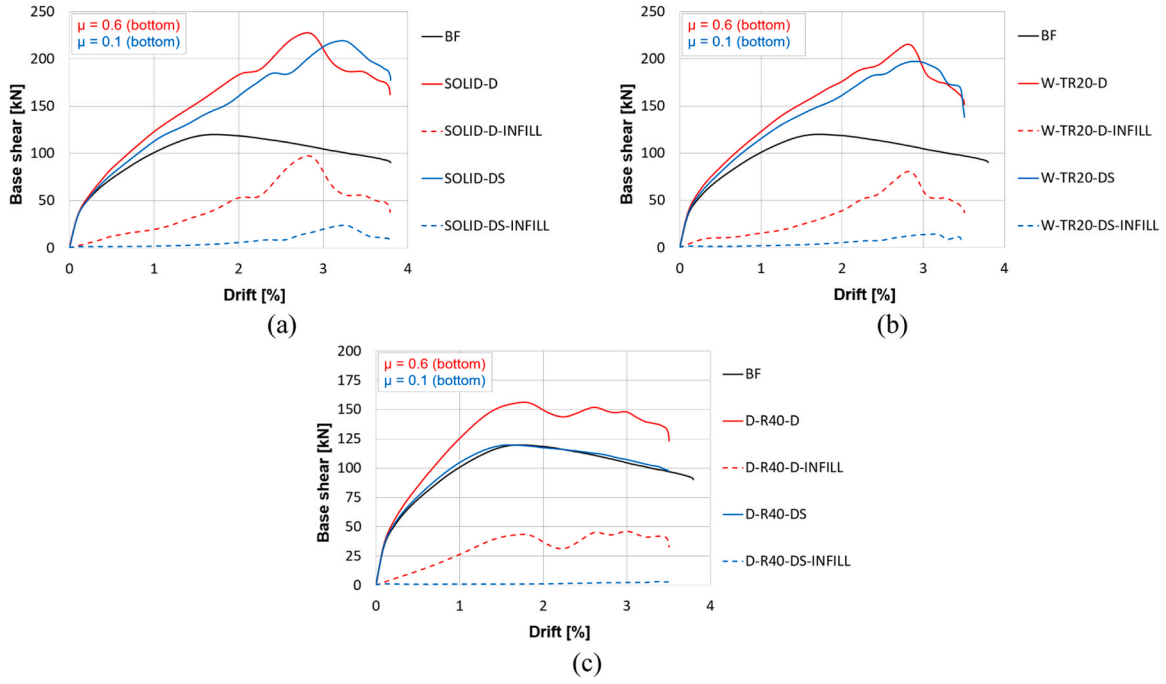

Fig. 14. Force-drift curves of decoupled infilled RC frames and decoupled masonry infills with different friction coefficients at the bottom interface for specimens: SOLID-D (a), W-TR20-D (b) and D-R40-D (c).

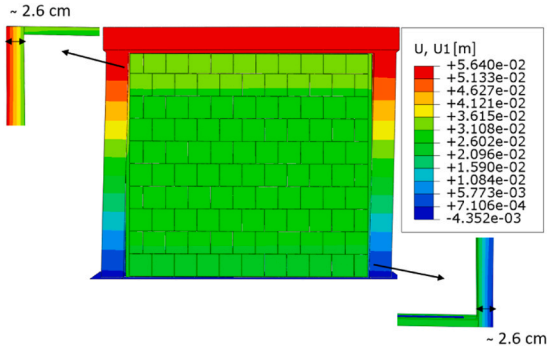

Fig. 15. Horizontal displacements plot and deformation of elastomeric strips at 2.0 % of in-plane drift – SOLID-DS.

the effective decoupling, the masonry infills exert minimal influence on the frame, which deforms and cracks similarly to a bare RC frame, as illustrated in Figs. 6, 8b, and 12a. Furthermore, the plastic hinges at the column ends are already formed at around 2.0 % of in-plane drift in all simulations, indicated by plastic strains in the reinforcement bars and compressive damage in the concrete (Fig. 16a,b). Moreover, this corresponds well with observations from the experimental test on the reference bare RC frame [60] as shown in Fig. 16c. Thus, decoupled infilled frames can achieve the deformation capacity of the bare frame, provided efficient decoupling is ensured through the design concept proposed in Chapter 6.2.

Following the definitions of the significant damage (SD) [59] and near collapse (NC) limit states [61], the SD limit state occurs at in-plane drifts above 2.3 %, while the NC limit state is not reached even beyond 2.5–3.0 % of in-plane drift. The decoupled infilled RC frames exhibit significant deformation reserves, with the SD limit state occurring beyond the maximum normative design in-plane drift of 2.0 % and the NC limit state shifted to higher in-plane drift levels.

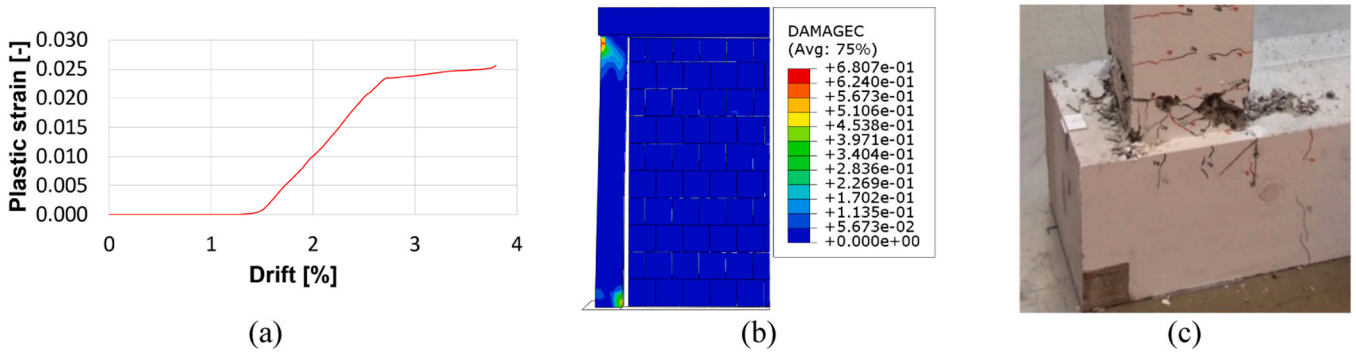

Fig. 16. Plastic strain for the reinforcement bar at the plastic hinge location (top-left corner) in simulation SOLID-D (a) and compressive damage propagation at 2.0 % of in-plane drift (b) and plastic hinge in bare frame test A [60] (c) at the ultimate in-plane drift of 3.5 %.

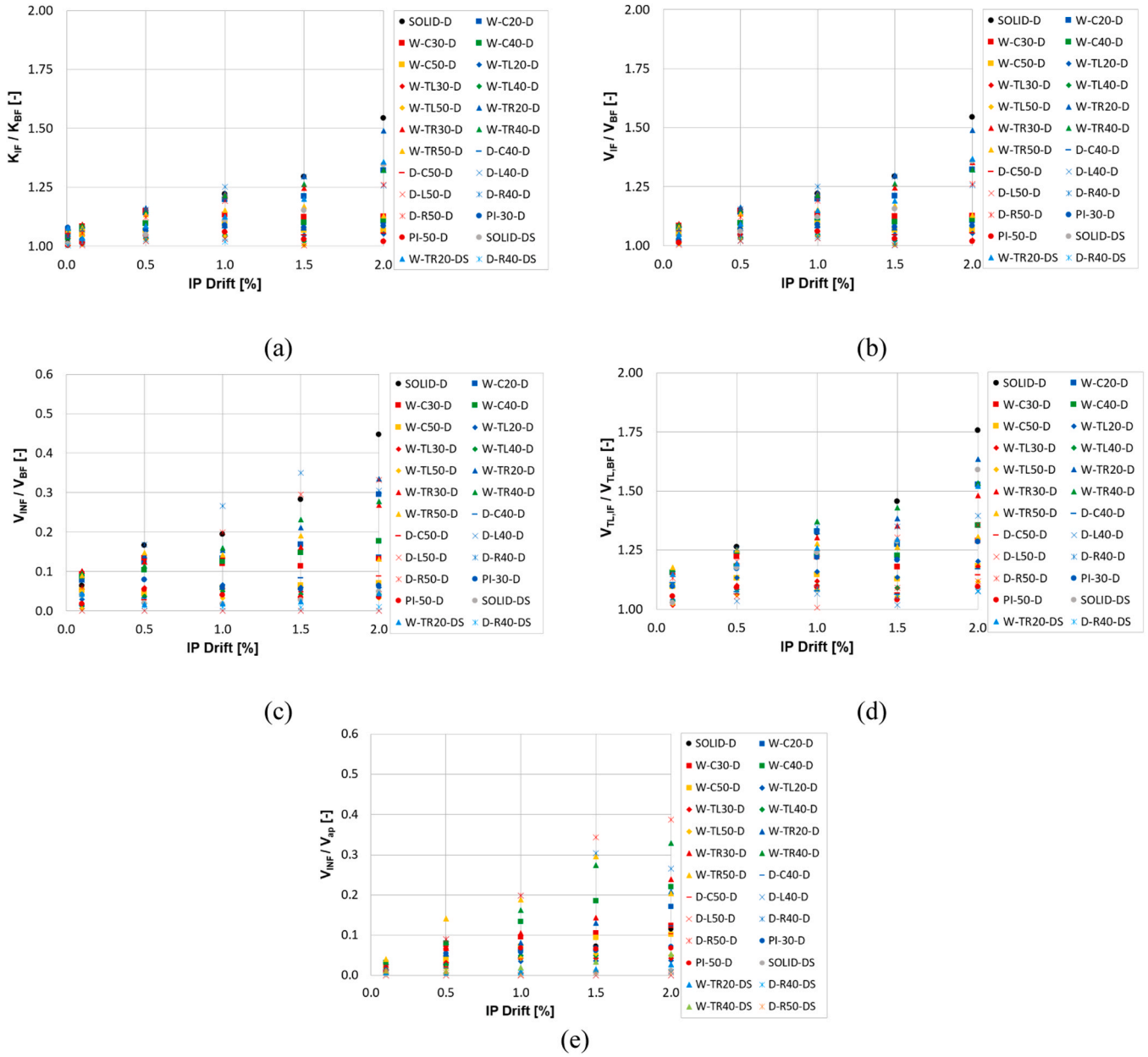

Fig. 17. K_{IF}/K_{BF} (a), V_{IF}/V_{BF} (b), V_{INF}/V_{BF} (c), $V_{TL,IF}/V_{BF}$ (d) and V_{INF}/V_{ap} (e) ratio for RC frames with decoupled masonry infills at different in-plane drifts.

5.2. Frame-infill interaction effects

The frame–infill interaction in RC frames with decoupled masonry infills is evaluated by comparing their in-plane response to that of the reference bare RC frame. Key design parameters include the ratio of in-plane stiffness of the infilled frame to the bare frame K_{IF}/K_{BF}, the ratio of base shear force of the infilled frame to that of the bare frame V_{IF}/V_{BF}, the ratio of base shear force of the masonry infill to that of the bare frame V_{INF}/V_{BF}, the ratio of shear force at the top of the left column (loaded corner) in the infilled frame to that in the bare frame $V_{TL,IF}/V_{TL,BF}$, and the ratio of base shear force of the masonry infill to the in-plane resistance in shear of masonry infill V_{INF}/V_{ap}. Results are evaluated up to the in-plane drift of 2.0 %.

First, the in-plane stiffness ratio K_{IF}/K_{BF} is evaluated. For small in-plane drift values, the initial in-plane stiffness is determined as the slope of the load-displacement curve within the linear range, prior to onset of nonlinear behaviour. At higher in-plane drift values the secant in-plane stiffness ratio is calculated. Fig. 17a shows that the initial in-plane stiffness of RC frames with decoupled masonry infills is nearly identical to that of the bare frame, regardless of opening size or location. Thus, the dynamic behaviour and horizontal forces of the frame remain essentially unchanged. With increasing in-plane drift values, the contribution of the masonry infill gradually increases, reaching maximum ratios greater than 1.3 at 2.0 % of in-plane drift only for the most unfavourable configurations SOLID-D, W-TR20-D and D-R40-D without sliding surface at the bottom. However, the incorporation of sliding surfaces at the bottom for these configurations effectively limits the K_{IF}/K_{BF} ratio to about 1.3, even at 2.0 % of in-plane drift. Fig. 17b demonstrates that the V_{IF}/V_{BF} ratio increases gradually with in-plane drift and their values are comparable to the stiffness ratios. Again, the installation of sliding surfaces at the bottom interface ensures that the V_{IF}/V_{BF} ratio is about 1.3 for the most unfavourable configurations at 2.0 % of in-plane drift. Fig. 17c shows a gradual, controlled increase in the V_{INF}/V_{BF} ratio with in-plane drift. The ratio exceeds 0.3 only in a few cases at 1.5 % and 2.0 % of in-plane drift with a sliding surface at the top. However, for configurations SOLID-D, W-TR20-D, and D-R40-D adding a bottom sliding surface reduces the V_{INF}/V_{BF} ratio below 0.05, even at 2.0 % of in-plane drift.

Fig. 17d shows that the shear force at the top-left (loaded) corner of infilled RC frames $V_{TL,IF}$ increases slightly with in-plane drift, while remaining close to that of bare frame $V_{TL,BF}$. The $V_{TL,IF}/V_{TL,BF}$ ratio stays below 1.3 for most cases at 1.5 % of in-plane drift and exceeds 1.5 only for a few configurations at 2.0 %. Chapter 6.2 introduces an equation to estimate the force transfer from the column to the masonry infill, ensuring effective decoupling. The force transfer in the frame corner is triangular and follows the global frame deformation. This distribution is used as a basis for the calculation of the contact force in Chapter 6.2.

Fig. 17e shows that the V_{INF}/V_{ap} ratio, representing the base shear of the decoupled masonry infill relative to its in-plane resistance in shear, remains below 0.3 for most cases. Herein, V_{ap} is calculated according to Eq. (11), without applying the partial safety factor γ_M. The ratio V_{INF}/V_{ap} exceeds the value of 0.3 only in a few configurations with a single top sliding surface (W-TR40-D,D-R40-D, D-R50-D) at in-plane drifts between 1.5 % and 2.0 %, while adding a bottom sliding surface further decreases the V_{INF}/V_{ap} ratio to below 0.05 for these cases.

6. Conclusions for the design of decoupled infilled RC frames

Based on the findings from the parametric study, a fundamental design concept for RC frames with INODIS-decoupled masonry infills is derived. As an input for the design of the decoupling system, the maximum interstorey in-plane drifts $d_{r,SD}$ are to be calculated at SD limit state using a simple bare frame model without considering the contribution of masonry infills. Using the calculated interstorey in-plane drift, the design can be carried out storey by storey for the most unfavourable masonry infill and the governing interstorey in-plane drift. Alternatively, the storey-by-storey approach can be omitted by assuming the maximum interstorey in-plane drift for all stories. The use of a bare frame model seems justified by the significantly reduced interaction between the frame and the masonry infill, as summarised in Chapter 5.2, and yields conservative interstorey in-plane drift values for design purposes, since only the frame stiffness is considered. Nevertheless, it must be verified that the contribution of the masonry infills to the lateral stiffness and resistance of the building against seismic actions can be neglected.

According to FprEN 1998–1–2:2025 [45], verification can be demonstrated by showing that the contribution of the masonry infills to the total lateral stiffness does not exceed 15 % of that provided by all primary seismic members. If the contribution is greater than 15 % but does not exceed 30 %, two separate analyses must be performed: one including only the primary members, and another including both the primary members and the masonry infills. In this case, the most unfavourable seismic action effects obtained from the two analyses should be considered in the verification. Alternatively, it shall be verified that the shear force transferred from the columns to the masonry infill is not greater than 30 % of its in-plane design resistance in shear. From the parametric study it can be concluded that the ratios K_{IF}/K_{BF} and V_{INF}/V_{ap} do not exceed 30 % for any masonry infill configuration with sliding surfaces at top and bottom interface, even at 2.0 % of in-plane drift. The results demonstrate that, with appropriate design, INODIS is generally capable of providing the required decoupling to classify decoupled masonry infills as non-interacting according to FprEN 1998–1–2:2025 [45]. Additional support for this conclusion lies in the fact that the RC frame columns in this study have the minimum typical dimensions used in practice b/h = 25/25 cm, while the masonry block thickness with 30 cm likely represents an upper bound of common practice. Consequently, the studied ratios would be expected to decrease for most practical configurations. Since the parametric study cannot be generalised, the following chapters present the design concept in which the transfer of shear force from the columns to the masonry infill is limited to 30 % of its in-plane design resistance in shear. Chapter 6.1 first explains the determination of the in-plane resistance of masonry infill, followed by the presentation of the overall design concept in Chapter 6.2.

6.1. In-plane resistance in shear of masonry infill

The in-plane resistance in shear of masonry infill is calculated based on frictional failure, as this generally provides the lowest shear resistance for masonry infills. Accordingly, the design in-plane resistance in shear of masonry infill $V_{ap,Rd}$ is calculated following the approach by [62], as recommended in [45], and reduced by the reduction factor ρ_{op} proposed by [63]:

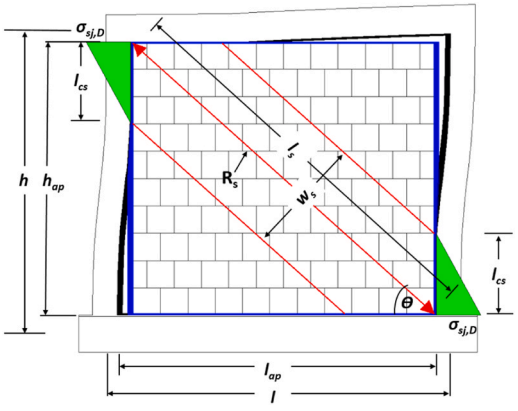

Fig. 18. Decoupled infilled RC frame deformation under lateral load and notations.

$$V_{\mathrm{ap,Rd}} = \frac{1}{\gamma_{\mathrm{M}}}\left[t_{ap}\quad f_{vk0}\left(l_{ap} + \mu_f \frac{l_s}{1-\mu_f \frac{h_{ap}}{l_{ap}}}\sin\theta\right)\right]\cdot\rho_{op} \tag{11}$$

Herein, γ_M is the partial safety factor at SD limit state, t_{ap} is the masonry infill thickness, l_{ap} masonry infill length, h_{ap} is the masonry infill clear height, l_s is the length of the diagonal of the masonry infill, θ is the angle between the masonry infill diagonal and the horizontal (beam), f_{vk0} is the characteristic initial shear strength of the masonry and μ_{f} is the characteristic friction coefficient. Fig. 18 shows the decoupled infilled RC frame with the notation of its dimensions. The reduction factor for openings is calculated as:

$$\rho_{op} = 0.55\exp(-0.035\cdot\alpha_a) + 0.44\exp(-0.025\cdot\alpha_1) \tag{12}$$

The coefficient α_{a} represents the ratio of the area of the opening to that of the masonry infill, and α_{l} is a ratio of the length of opening to the masonry infill length. However, it should be noted that the design in-plane resistance in shear of masonry infill, $V_{ap,Rd}$, calculated according to Eq. (11) and adjusted by the reduction factor for openings in Eq. (12), does not necessarily represent the actual failure mode of decoupled masonry infill. Instead, this approach provides a conservative approximation that accounts for the influence of openings on the in-plane resistance of masonry infills.

6.2. Design concept

It must be verified that the shear force $V_{c,ap}$ transferred from the columns to the masonry infill does not exceed 30 % of the in-plane design resistance in shear $V_{ap,Rd}$ of the masonry infill:

$$V_{\mathrm{c,ap}} \le 0.3V_{\mathrm{ap,Rd}} \tag{13}$$

The shear force $V_{c,ap}$ transferred from the columns to the masonry infill can be calculated as:

$$V_{c,ap} = \sigma_{sj,D}\cdot t_{ap}\cdot l_{cs} \tag{14}$$

Here $\sigma_{sj,D}$ is the design average stress of the decoupling material along the contact length l_{cs}. The contact length, shown in Fig. 18, can be calculated as:

$$l_{cs} = w_s/\cos\Theta \tag{15}$$

where w_s is the width of the strut, also shown in Fig. 18, and calculated according to [62]:

$$w_s = 0.25l_s = 0.25l_{ap}/\cos\Theta \tag{16}$$

The design average stress $\sigma_{sj,D}$ is calculated assuming a triangular stress distribution along the contact length, as shown in Fig. 18. The maximum stress of this distribution at the top of the masonry infill is determined from the stress–strain curve of the decoupling material, corresponding to the strain at the design interstorey in-plane drift $d_{\mathrm{r,SD}}$. If INODIS is installed with sliding interfaces at both the top and bottom, the design in-plane drift can be reduced by 50 %, as vertical elastomeric strips at both sides of the masonry infill are activated. If the shear force $V_{c,ap}$ exceeds 30 % of the in-plane design resistance in shear of masonry infill $V_{ap,Rd}$, the thickness and/or stiffness of the vertical elastomeric strips need to be adjusted. Another option is to reduce the design interstorey in-plane drift $d_{r,SD}$ by modifying the structural system. Finally, once the condition is satisfied, the seismic design can be further carried out, without considering masonry infills and using only the bare frame model. The flow chart of the design procedure is shown in Fig. 19.

7. Conclusions

This article presents the results of the numerical study on the in-plane behaviour of RC frames with decoupled masonry infills. Decoupled masonry infills are separated from the RC frame using the innovative decoupling system INODIS presented by [44]. The study employs the numerical model developed by [15], which is based on a simplified micro-modelling approach. First, the numerical model is validated against three in-plane experimental tests. Afterwards, it is employed for an extensive parametric study, varying the type, size and location of openings in the masonry infill. In addition to masonry infills with window and full-height door openings, the study considers partially infilled RC frames.

The results of the parametric study demonstrate that the proposed decoupling system effectively decouples masonry infills from RC frames across all configurations. Although masonry infills display different deformation mechanisms depending on the opening configuration, the decoupling system efficiently accommodates the deformation of the surrounding RC frame in all cases. Therefore, the activation level of the decoupled masonry infills remains negligible up to the maximum design in-plane drift of 2.0 %. Even when masonry infills are activated, at in-plane drifts above 2.0 %, the activation is slow and controlled, with a gradual increase of the base shear forces taken by the masonry infills. Moreover, these forces can be reduced by a factor greater than 4 if the sliding profiles are installed at both the top and bottom frame-infill interface. As a result of the efficient decoupling, the first cracking in the decoupled masonry infills typically occurs at in-plane drifts exceeding the maximum design in-plane drift of 2.0 %, while the significant damage (SD) limit state develops at in-plane drifts above 2.3 %. The decoupled masonry infills can still accommodate in-plane drifts of 2.5–3.0 % without total damage.

The effective decoupling allows RC frames with decoupled masonry infills to deform and crack as the reference bare RC frame. The force-

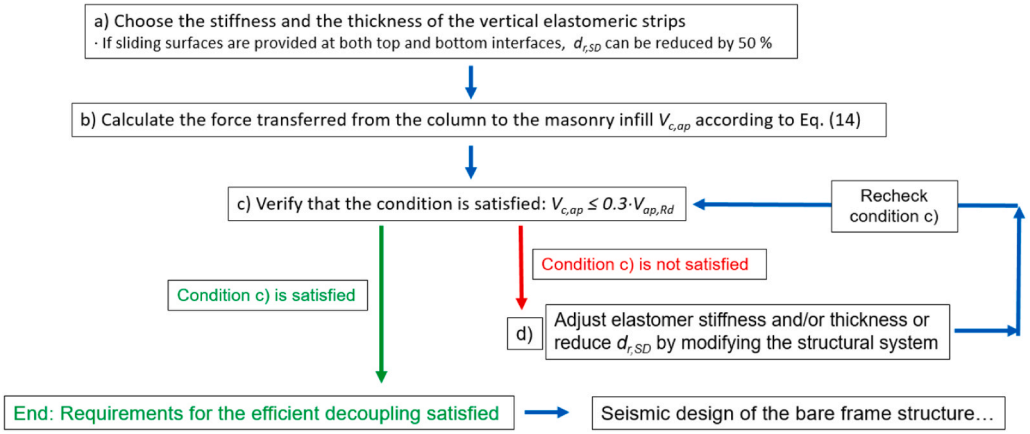

Fig. 19. Design procedure for verification of the efficient decoupling.

drift response of decoupled infilled RC frames closely matches that of the reference bare RC frame, particularly up to the maximum design in-plane drift of 2.0 %. In addition, the distribution of bending moments in the columns of the decoupled infilled RC frames remains practically unchanged compared to the case of the reference bare RC frame. For several configurations, column shear forces at loaded corners increase slightly for in-plane drifts above 0.5 %. However, this increase is negligible, as the ratio of the column shear force at the top-left corner of the decoupled infilled RC frame to that of the bare RC frame generally remains below 1.3 at 1.5 % of in-plane drift and exceeds 1.5 at the maximum design in-plane drift of 2.0 % only in a few cases.

The key finding of the study is that the application of the innovative decoupling system INODIS ensures that the frame-infill interaction remains negligible for all configurations in the parametric study, up to the in-plane drift of 2.0 %, which represents the upper limit for a highly ductile design of RC frame structure. Therefore, according to FprEN 1998–1–2:2025 [45], the investigated masonry infills can be classified as non-interacting, allowing the use of simplified verification rules. Based on the findings of the study and the recommendations of FprEN 1998–1–2:2025 [45], a simple design concept is proposed. It suggests that an RC frame with a decoupled masonry infill can be designed as a corresponding bare RC frame, provided that the shear force transferred from the column to the masonry infill does not exceed 30 % of the in-plane design resistance in shear of the masonry infill. If this condition is satisfied, masonry infill activation remains low, with negligible impact on the dynamic characteristics of the RC frame structure (initial and secant stiffness), as well as on the internal forces in the columns, which justifies the seismic design of the bare frame structure. This straightforward design approach offers practical means to enhance the seismic safety of RC frame structures with masonry infills.

Throughout the present study and previous experimental research by the authors [44], the application of the decoupling system has been shown to be an effective solution for protecting masonry infills and surrounding RC frames from seismic damage. Moreover, decoupling of masonry infills from RC frames should prevent any adverse effects of masonry infills on the global behaviour of RC frame structures. Therefore, the application of the decoupling system should allow flexibility when planning the distribution of masonry infills within the buildings. In addition, the proposed design concept enables the practical implementation of the decoupling system, ensuring effective isolation and allowing seismic design of the bare frame structure. The plan for the future work is to demonstrate the application of the proposed design concept on a practical example.

CRediT authorship contribution statement

Aleksa Milijaš: Conceptualization, Methodology, Validation, Formal analysis, Visualization, Investigation, Data Curation, Writing - Original draft preparation, Writing - Reviewing and Editing. **Marko Marinković:** Conceptualization, Methodology, Validation, Investigation, Writing - Reviewing and Editing, Supervision. **Christoph Butenweg:** Conceptualization, Methodology, Validation, Investigation, Writing - Reviewing and Editing, Funding acquisition, Supervision. **Sven Klinkel:** Writing - Reviewing and Editing, Supervision.

Funding

This work was supported by the AiF Project (Grant no: 20912 N/2, Christoph Butenweg) “Development of an innovative approach for decoupling masonry infills and non-load-bearing masonry walls from the load-bearing structure”.

Declaration of Competing Interest

The authors declare that they have no known competing financial interests or personal relationships that could have appeared to influence the work reported in this paper.

Data availability

Data will be made available on request.

References

[1] Marinković M, Baballëku M, Isufi B, Blagojević N, Milićević I, Brzev S. Performance of RC cast-in-place buildings during the November 26, 2019 Albania earthquake. Bull Earthq Eng 2022;20:5427–80. https://doi.org/10.1007/s10518-022-01414-y.
[2] Vicente RS, Rodrigues H, Varum H, Costa A, da Silva JARM. Performance of masonry enclosure walls: lessons learned from recent earthquakes. Earthq Eng Eng Vib 2012;11(1):23–34. https://doi.org/10.1007/s11803-012-0095-3.
[3] Perrone D, Calvi PM, Nascimbene R, Fischer EC, Magliulo G. Seismic performance of non-structural elements during the 2016 Central Italy earthquake. Bull Earthq Eng 2019;17(10):5655–77. https://doi.org/10.1007/s10518-018-0361-5.
[4] Demir A, Celebi E, Ozturk H, Ozcan Z, Ozocak A, Bol E, Sert S, Zehra S, Arslan E, Yaman Z, Utkucu M, Mert N. Destructive impact of successive high magnitude earthquakes occurred in Türkiye’s Kahramanmaraş on February 6, 2023. Bull Earthq Eng 2024:1–27. https://doi.org/10.1007/s10518-024-01865-5.
[5] Milijaš A, Marinković M, Butenweg C, Klinkel S. Experimental results of reinforced concrete frames with masonry infills with and without openings under combined quasi-static in-plane and out-of-plane seismic loading. Bull Earthq Eng 2023;21:3537–79. https://doi.org/10.1007/s10518-023-01664-4.
[6] Mehrabi AB, Shing PB, Schuller MP, Noland JL. Experimental evaluation of masonry-infilled RC frames. J Struct Eng 1996;122(3):228–37. https://doi.org/10.1061/(ASCE)0733-9445(1996)122:3(228).
[7] Alwashali H, Sen D, Jin K, Maeda M. Experimental investigation of influences of several parameters on seismic capacity of masonry infilled reinforced concrete frame. Eng Struct 2019;189:11–24. https://doi.org/10.1016/j.engstruct.2019.03.020.
[8] Stylianidis KC. Experimental investigation of masonry infilled RC frames. Open Constr Build Technol J 2012;6(1):194–212. https://doi.org/10.2174/1874836801206010194.
[9] Chiou TC, Hwang SJ. Tests on cyclic behavior of reinforced concrete frames with brick infill. Earthq Eng Struct Dyn 2015;44(12):1939–58. https://doi.org/10.1002/eqe.2564.
[10] Huang H, Burton HV, Sattar S. Development and utilization of a database of infilled frame experiments for numerical modeling. J Struct Eng 2020;146(6):04020079. https://doi.org/10.1061/(ASCE)ST.1943-541X.0002608.
[11] Dias-Oliveira J, Rodrigues H, Asteris PG, Varum H. On the seismic behavior of masonry infilled frame structures. Buildings 2022;12(8):1146. https://doi.org/10.3390/buildings12081146.
[12] Marinković M. Innovative system for seismic resistant masonry infills in reinforced concrete frame structures. Faculty of Civil Engineering. Belgrade: University of Belgrade; 2018.
[13] Zhai C, Kong J, Wang X, Chen Z. Experimental and finite element analytical investigation of seismic behavior of full-scale masonry infilled RC frames. J Earthq Eng 2016;20(7):1171–98. https://doi.org/10.1080/13632469.2016.1138171.
[14] Nasiri E, Liu Y. Development of a detailed 3D FE model for analysis of the in-plane behaviour of masonry infilled concrete frames. Eng Struct 2017;143:603–16. https://doi.org/10.1016/j.engstruct.2017.04.049.
[15] Marinković M, Butenweg C. Numerical analysis of the in-plane behaviour of decoupled masonry infilled RC frames. Eng Struct 2022;272:114959. https://doi.org/10.1016/j.engstruct.2022.114959.
[16] Asteris PG. Lateral stiffness of brick masonry infilled plane frames. J Struct Eng 2003;129(8):1071–9. https://doi.org/10.1061/(ASCE)0733-9445(2003)129:8(1071).
[17] D’Ayala D, Worth J, Riddle O. Realistic shear capacity assessment of infill frames: comparison of two numerical procedures. Eng Struct 2009;31(8):1745–61. https://doi.org/10.1016/j.engstruct.2009.02.044.
[18] Milanesi R, Morandi P, Magenes G. Local effects on RC frames induced by AAC masonry infills through FEM simulation of in-plane tests. Bull Earthq Eng 2018;16:4053–80. https://doi.org/10.1007/s10518-018-0353-5.
[19] Mohebkhah A, Tasnimi AA, Moghadam HA. Nonlinear analysis of masonry-infilled steel frames with openings using discrete element method. J Constr Steel Res 2008;64(12):1463–72. https://doi.org/10.1016/j.jcsr.2008.01.016.
[20] Chen Z, Zhou Y, Kinoshita T, DeJong MJ. Distinct element modeling of the in-plane and out-of-plane response of ordinary and innovative masonry infill walls. Structures 2023;50:1447–60. https://doi.org/10.1016/j.istruc.2023.02.035.
[21] Stavridis A, Shing PB. Finite-element modeling of nonlinear behavior of masonry-infilled RC frames. J Struct Eng 2010;136(3):285–96. https://doi.org/10.1061/(ASCE)ST.1943-541X.116.
[22] Di Trapani F, Di Benedetto M, Petracca M, Camata G. Local infill-frame interaction under seismic loads: Investigation through refined micro-modeling. Eng Struct 2024;315:118088. https://doi.org/10.1016/j.engstruct.2024.118088.
[23] Di Trapani F, Tomaselli G, Cavaleri L, Bertagnoli G. Macroelement model for the progressive-collapse analysis of infilled frames. J Struct Eng 2021;147(6):04021079. https://doi.org/10.1061/(ASCE)ST.1943-541X.0003014.
[24] Liberatore L, Noto F, Mollaioli F, Franchin P. In-plane response of masonry infill walls: comprehensive experimentally based equivalent strut model for

deterministic and probabilistic analysis. Eng Struct 2018;167:533–48. https://doi.org/10.1016/j.engstruct.2018.04.057.
[25] Žarnić R, Tomažević M. An Experimentally Obtained Method for Evaluation of the Behaviour of Masonry Infilled R/C Frames, VI. Tokyo, Japan: Proceedings of the 9th World Conference on Earthquake Engineering; 1988. p. 163–8.
[26] Al-Chaar G. Evaluating strength and stiffness of unreinforced masonry infill structures (No.ERDC/CERL-TR-02–1). Eng Res Dev Cent Champaign il Constr Eng Res Lab 2002.
[27] Chrysostomou CZ, Asteris PG. On the in-plane properties and capacities of infilled frames. Eng Struct 2012;41:385–402. https://doi.org/10.1016/j.engstruct.2012.03.057.
[28] El-Dakhakhni WW, Elgaaly M, Hamid AA. Three-strut model for concrete masonry-infilled steel frames. J Struct Eng 2003;129(2):177–85. https://doi.org/10.1061/(ASCE)0733-9445(2003)129:2(177).
[29] Basha S, Kaushik H. Investigation on improving the shear behavior of columns in masonry infilled RC frames under lateral loads. Bull Earthq Eng 2019;17:3995–4026. https://doi.org/10.1007/s10518-019-00622-3.
[30] Wararuksajja W, Srechai J, Leelataviwat S. Seismic design of RC moment-resisting frames with concrete block infill walls considering local infill-frame interactions. Bull Earthq Eng 2020;18:6445–74. https://doi.org/10.1007/s10518-020-00942-9.
[31] MSJC (2013) – ACI 530–13/ASCE 5–13/TMS 402–13. Building Code Requirements for Masonry Structures. United States: Masonry Standards Joint Committee.
[32] FEMA 306 (1998). Evaluation of Earthquake damaged concrete and masonry wall buildings. Applied Technology Council (ATC-43 project), 555 Twin Dolphin Drive, suite 550, Redwood city, California, USA.
[33] Asteris PG, Costovos DM, Chrysostomou CZ, Mohebkhah A, Al-Chaar GK. Mathematical micromodeling of infilled frames: state of the art. Eng Struct 2013;56:1905–21. https://doi.org/10.1016/j.engstruct.2013.08.010.
[34] Bhat ZM, Singh Y, Agarwal P. Cyclic testing and diagonal strut modelling of different types of masonry infills in reinforced concrete frames design for modern codes. Eng Struct 2024;317:118695. https://doi.org/10.1016/j.engstruct.2024.118695.
[35] Tsantilis AV, Triantafillou TC. Innovative seismic isolation of masonry infills using cellular materials at the interface with the surrounding RC frames. Eng Struct 2018;155:279–97. https://doi.org/10.1016/j.engstruct.2017.11.025.
[36] Tsantilis AV, Triantafillou TC. Innovative seismic isolation of masonry infills in steel frames using cellular materials at the frame-infill interface. J Earthq Eng 2018;24(11):1729–46. https://doi.org/10.1080/13632469.2018.1478347.
[37] GB 50011-2010 (2010) Code for Seismic Design of Buildings, Architecture & Building Press, Beijing, China (In Chinese).
[38] Standards New Zealand (2004) NZS 4230:2004, Design of Reinforced Concrete Masonry Structures, Standards. New Zealand, Wellington, New Zealand.
[39] Kuang JS, Wang Z. Cyclic load tests of RC frame with column-isolated masonry infills. Istanbul: Second European conference on earthquake engineering and seismology; 2014. p. 25–9.
[40] Marinković M, Butenweg C. Experimental testing of decoupled masonry infills with steel anchors for out-of-plane support under combined in-plane and out-of-plane seismic loading. Constr Build Mater 2022;318:126041. https://doi.org/10.1016/j.conbuildmat.2021.126041.
[41] Jin W, Zhai C, Kong J, Liu W, Zhang M. In-plane and out-of-plane quasi-static tests on RC frames with a new type of frame-isolated infills. Eng Struct 2021;246:113079. https://doi.org/10.1016/j.engstruct.2021.113079.
[42] Jin W, Zhai C, Zhang M, Liu W, Wei Y, Xie L. Experimental investigation on the in-plane and out-of-plane interaction of isolated infills in RC frames. Eng Struct 2023;293:116569. https://doi.org/10.1016/j.engstruct.2023.116569.
[43] Marinković M, Butenweg C. Innovative decoupling system for the seismic protection of masonry infill walls in reinforced concrete frames. Eng Struct 2019;197:109435. https://doi.org/10.1016/j.engstruct.2019.109435.
[44] Milijaš A, Marinković M, Butenweg C, Klinkel S. Experimental investigation on the seismic performance of reinforced concrete frames with decoupled masonry infills: considering in-plane and out-of-plane load interaction effects. Bull Earthq Eng 2024;22:7489–546. https://doi.org/10.1007/s10518-024-02012-w.
[45] FprEN 1998-1-2: 2025, Eurocode 8: Design of structures for earthquake resistance – Part 1-2: Buildings, CEN, N1396, TC250/SC8, Brussels.
[46] Tasnimi AA, Mohebkhah A. Investigation on the behavior of brick-infilled steel frames with openings, experimental and analytical approaches. Eng Struct 2011;33(3):968–80. https://doi.org/10.1016/j.engstruct.2010.12.018.
[47] Mansouri A, Marefat MS, Khanmohammadi M. Experimental evaluation of seismic performance of low-shear strength masonry infills with openings in reinforced concrete frames with deficient seismic details. Struct Des Tall Spec Build 2014;23(15):1190–210. https://doi.org/10.1002/tal.1115.
[48] Dassault Systemes: Abaqus/CAE. 2019 – Software.
[49] Simulia, Abaqus, User Manual. Version 6.13. Providence, RI, USA: DS SIMULIA Corp., 2013. URL ⟨https://www.3ds.com/products-services/simulia/products/abaqus/⟩.
[50] Mehrabi AB, Shing PB. Finite element modelling of masonry-infilled RC frames. J Structural Engineering. NY 1997;123(5):604–13.
[51] Kaushik H, Rai D, Jain S. Stress-strain characteristics of clay brick masonry under uniaxial compression. J Mater Civ Eng 2007;19(9):728–39. https://doi.org/10.1061/(ASCE)0899-1561(2007)19:9(728).
[52] Milijaš A, Marinković M, Butenweg C, Klinkel S. In-plane behaviour of RC frames with traditional and decoupled infills: Parametric study. Proceedings of the 3rd Croatian Conference on Earthquake Engineering-3CroCEE Split; 2025. https://doi.org/10.5592/CO/3CroCEE.2025.96.
[53] Lopez-Almansa F, Alfarah B, Oller S. Numerical simulation of RC frame testing with damaged plasticity model. Comparison with simplified models. Istanbul, Turkey: Second European conference on Earthquake Engineering and Seismology; 2014. https://doi.org/10.13140/2.1.3457.2169.
[54] Lee J, Fenves GL. Plastic-damage model for cyclic loading of concrete structures. J Eng Mech 1998;124(8):892–900.
[55] Tubaldi E, et al. Shake table testing of masonry-infilled RC frames with flexible joints for seismic-resilient structural performance. International Workshop in Engineering Research Infrastructures for European Synergies. Cham: Springer Nature Switzerland; 2025. p. 144–58. https://doi.org/10.1007/978-3-031-98893-6_15.
[56] Nazir S, Dhanasekar M. A non-linear interface element model for thin layer high adhesive mortared masonry. Comput Struct 2014;144:23–39. https://doi.org/10.1016/j.compstruc.2014.07.023.
[57] Benzeggagh MI, Kenane M. Measurement of mixed-mode delamination fracture toughness of unidirectional glass/epoxy composites with mixed-mode bending apparatus. Compos Sci Technol 1996;56(4):439–49. https://doi.org/10.1016/0266-3538(96)00005-X.
[58] Schlussbericht zu IGF-Vorhaben Nr. 20912N,Entwicklung eines innovativen Ansatzes zur Entkopplung von Ausfachungen und nicht tragenden Trennwänden aus Mauerwerk von der Tragstruktur“, Forschungsvereinigung Ziegelindustrie e.V., Reinhardtstraße 12-16, 10117 Berlin.
[59] Morandi P, Hak S, Magenes G. Performance-based interpretation of in-plane cyclic tests on RC frames with strong masonry infills. Eng Struct 2018;156:503–21. https://doi.org/10.1016/j.engstruct.2017.11.058.
[60] Butenweg C, Marinković M, Salatić R. Experimental results of reinforced concrete frames with masonry infills under combined quasi-static in-plane and out-of-plane seismic loading. Bull Earthq Eng 2019;17(6):3397–422. https://doi.org/10.1007/s10518-019-00602-7.
[61] Sassun K, Sullivan TJ, Morandi P, Cardone D. Characterising the in-plane seismic performance of infill masonry. ISSN: 11749857 Bull NZ Soc Earthq Eng 2016;49(1):100–17. https://doi.org/10.5459/bnzsee.49.1.98-115.
[62] Paulay T, Priestley MN. Seismic design of reinforced concrete and masonry buildings, 768. New York: Wiley; 1992.
[63] Decanini LD, Liberatore L, Mollaioli F. Strength and stiffness reduction factors for infilled frames with openings. Earthq Eng Eng Vib 2014;13:437–54. https://doi.org/10.1007/s11803-014-0254-9.